Review—Copper Oxide-Based Ternary and Quaternary Oxides: Where Solid-State Chemistry Meets Photoelectrochemistry

Krishnan Rajeshwar, [1,*,z] Mohammad Kabir Hossain,[1,**] Robin T. Macaluso,[1] Csaba Janáky,[2,3] Andras Varga,[2,3] and Pawel J. Kulesza[4,***]

[1]*Department of Chemistry & Biochemistry, The University of Texas at Arlington, Arlington, Texas 76109-0065, USA*
[2]*MTA-SZTE, Lendület Photoelectrochemistry Research Group, Szeged H-6720, Hungary*
[3]*Department of Physical Chemistry and Materials Science, University of Szeged, Szeged H-6720, Hungary*
[4]*Faculty of Chemistry, University of Warsaw, PL-02-093 Warsaw, Poland*

This review article addresses areas where solid-state chemistry concepts can contribute to the on-going search for a "magic bullet" inorganic semiconductor that can efficiently split water or reduce CO_2. First, a methodology to visualize complex ternary oxide combinations is outlined using 31 examples based on copper in both +1 and +2 oxidation states. Then the synthetic aspects are reviewed followed by a discussion of the structural characteristics. The optoelectronic aspects are considered next, culminating the review with the state-of-the-art in the practical applicability of these materials in solar fuels photogeneration and environmental (e.g., azo dye) remediation.

This review article addresses the nexus between two seemingly disparate disciplines, namely solid-state chemistry (SSC) and photoelectrochemistry (PEC) using copper-based complex (ternary and quaternary) oxides as a discussion framework. The two disciplines, SSC and PEC, have more or less developed in a parallel fashion since their halcyon days in the mid-1970s. Both SSC and PEC shared an interest in similar materials (mainly oxides and chalcogenides) but for rather different applications. While SSC has focused mainly on magnetic or electronically and ionically conductive solid materials, and eventually evolving to superconducting (so-called high T_c) materials, PEC has dealt mainly with inorganic *semiconductors*. However, and interestingly enough, the two disciplines have coalesced in the area of energy conversion. The past couple decades have thus witnessed remarkable advances in the development of solid-state materials for Li-ion batteries, thermoelectric conversion, photovoltaic solar cells, and solid-oxide fuel cells. Even high T_c-superconductivity studies have translated to niche applications in practical technologies. However, in spite of a comparably early history of study, solar fuels (e.g., water splitting, CO_2 reduction, N_2 reduction) have not seen the light of day in terms of commercialization.

One may well argue that we lack a "magic bullet" inorganic semiconductor that can split water or reduce CO_2 in a stable, sustainable, and efficient manner because the connection between SSC and PEC has only occurred in fits and starts. With the entry of (a veritable melting pot of) scientists from a wide variety of technical backgrounds (e.g., colloid chemistry, ultrafast spectroscopy, solid-state physics, electrochemistry, etc.) into the PEC field, it was only natural that the emphasis on solid state *chemistry* has been somewhat diluted. For example, while the early history of PEC is liberally sprinkled with studies from solid-state research groups (see Refs. 1–4 as random examples), instances in the post 1990 s where SSC concepts have been *rationally* and *deliberately* applied, are sporadic,[5,6] as further discussed below.

Scope of Review and Literature Precedence

This review refocuses the key role that solid-state chemistry can play in the continuing search for an inorganic semiconductor (or a combination of semiconductors) for solar fuels photogeneration. First, means of visualizing complex oxide chemical compositions are introduced via suitable diagrams. Next, the synthetic aspects are considered followed by a review of the structural aspects of copper oxide-based ternary and quaternary oxides starting with the parent oxides, copper(I) oxide and copper(II) oxide (Cu_2O and CuO). The optoelectronic attributes are discussed in turn, culminating in an examination of the extent to which these new materials have met the needs for applicability in the solar fuels and environmental remediation arenas.

We are not aware of a similar, overarching review on this topic although copper(I)-based *p*-type oxides were recently reviewed for photoelectrochemical and photovoltaic solar energy conversion applications.[6] Tantalum- and niobium-based ternary oxides were discussed in this particular article, as were four copper(I) delafossites and two Cu-V-O oxides (Cu_3VO_4 and $Cu_2V_3O_8$).[6] Areas where the present article overlaps with this precedent review are identified later. The synthetic aspects of ternary metal oxide nanostructures have been reviewed[7] as were their applications in supercapacitors.[8] While not focusing per se on solar fuels generation, three recent articles[9–11] may be cited that share a similar objective to the present review: namely, *targeted* materials development for a specific application. Thus, we note a recent article that discusses how simple chemical concepts can be turned into viable strategies for thermoelectric materials development.[9]

Another article[10] focuses on the accuracy of density functional theory in predicting the formation energetics of ternary oxides from their binary oxide counterparts. Finally, ab initio global structural prediction, and specifically the minima hopping method, was used to study 183 different compositions of the form, MXO_2, where M = Cu, Ag, or Au (coinage metal), and X is an element in the Periodic Table.[11] The application target in this particular study was *p*-type transparent conducting oxide (TCO) development.[11] While the materials' application focus in the present discussion is mostly on solar water splitting, closely allied technology aspects related to photoelectrochemical CO_2 reduction and heterogeneous photocatalytic environmental remediation are also peripherally addressed, for the sake of completeness. It is worth noting that the photocatalysis application has seen the light of day, in terms of commercial realization, sooner than the other applications.

Tables Ia and Ib summarize the oxide candidates considered in the present review article; the two compilations relate to compounds based on copper in the +1 and +2 oxidation states respectively.

Table I. Copper oxide-based ternary oxides considered in this review. a) Copper(I) oxide-based. b) Copper(II) oxide-based.

No.	Ternary Oxide	A oxide	B oxide	A oxide: B oxide	Ref(s).
	a) Copper(I) oxide-based				
1	$CuAlO_2$	Cu_2O	Al_2O_3	1: 1	12–15
2	$CuCrO_2$		Cr_2O_3	1: 1	16,17
3	$CuFeO_2$		Fe_2O_3	1: 1	5,18–21
4	α-$CuGaO_2$		Ga_2O_3	1: 1	22–26
5	β-$CuGaO_2$		Ga_2O_3	1: 1	27,28
6	$CuNbO_3$		Nb_2O_5	1: 1	29,30
7	$CuNb_3O_8$		Nb_2O_5	1: 3	31,32
8	$Cu_2Nb_8O_{21}$		Nb_2O_5	1: 4	33
9	$CuRhO_2$		Rh_2O_3	1: 1	34
10	α-$Cu_2Ta_4O_{11}$		Ta_2O_5	1: 2	35
11	β-$Cu_2Ta_4O_{11}$		Ta_2O_5	1: 2	36
12	$Cu_3Ta_7O_{19}$		Ta_2O_5	3: 7	37,38
13	$Cu_5Ta_{11}O_{30}$		Ta_2O_5	5: 11	37,39
14	Cu_3VO_4		V_2O_5	3: 1	40
	b) Copper(II) oxide-based				
1	$CuAl_2O_4$	CuO	Al_2O_3	1: 1	41–44
2	$CuBi_2O_4$		Bi_2O_3	1: 1	45–56
3	$CuCo_2O_4$		Co_2O_3	1: 1	44,57–59
4	$CuCr_2O_4$		Cr_2O_3	1: 1	44,60–66
5	$CuFe_2O_4$		Fe_2O_3	1: 1	44,67–69
6	$CuGa_2O_4$		Ga_2O_3	1: 1	70
7	$CuMn_2O_4$		Mn_2O_3	1: 1	44,71
8	$CuMoO_4$		MoO_3	1: 1	72,73
9	$CuNb_2O_6$		Nb_2O_5	1: 1	74
10	$Cu_3Nb_2O_8$		Nb_2O_5	3: 1	75
11	CuV_2O_6		V_2O_5	1: 1	76–78
12	α-$Cu_2V_2O_7$		V_2O_5	2: 1	79
13	β-$Cu_2V_2O_7$		V_2O_5	2: 1	76,77,79
14	β-$Cu_3V_2O_8$		V_2O_5	3: 1	80–83
15	γ-$Cu_3V_2O_8$		V_2O_5	3: 1	79,84
16	$Cu_{11}V_6O_{26}$		V_2O_5	11: 3	79,85
17	$CuWO_4$		WO_3	1: 1	86–94

Figures 1a and 1b illustrate the materials' scope from a Periodic Table perspective.

Visualizing Ternary and Quaternary Oxide Compositions and Their Relationship to the Binary Oxide Components

In this paper, A, B, and C represent metal cations in a ternary or quaternary oxide compound. Of course, for the present discussion, A = Cu in all the cases. At first glance, the various oxide compositions in Tables Ia and Ib appear to be complicated in terms of the combinations of formula subscripts, especially in the Cu-Nb-O, Cu-Ta-O, and Cu-V-O cases. However, a simple way to visualize these is to break up each ternary compound into a combination of the component binaries. Thus the two binaries are shown in columns 3 and 4 of Tables Ia and Ib and their combining ratios is shown in column 5 in each case. Thus the vast majority of the compounds considered are rather simple 1:1 molar combinations, although combinations such as 11:3 are observed in the Cu-V-O systems. Polymorphs of the same compound are also observed in many cases (designated in Tables Ia and Ib by α, β, etc.) and they will be further considered in the section below on structural aspects.

A final point to note is that the prescribed visualization of ternary compounds as combinations of corresponding binaries, is by no means, unique to oxides. This approach works equally well for non-oxides, e.g., chalcogenides, phosphides, arsenides etc. By extrapolation, quaternary compounds may be visualized as derived from the component binaries in the same manner. Thus, the quaternary compound, $AgBiW_2O_8$, studied by one of us recently,[95] is really a 1:1:4 combination of the three component oxides, namely, Ag_2O, Bi_2O_3, and WO_3. Certainly, this is not readily apparent from the above formula! Other Cu-based quaternary compounds are considered below.

Phase diagrams can also represent thermodynamically stable ternary and quaternary compounds based on their simpler components; this is depicted in Figure 2. The generic ternary phase diagram is shown in Figure 2a and a specific Cu-Bi-V-O system is considered in Figure 2b. Consider Figure 2a first. Each corner of the (equilateral) triangle represents 100% of one component (i.e., a binary compound). Points along each edge of the equilateral triangle represent a combination of two binaries on either end of the triangle. Any point on the edge must follow the lever rule; for example, the mid-point constitutes the 1:1 ternary compound, and AB_2O_x is represented as a point that is located 1/3 of the length toward the corner labeled "A-oxide" and 2/3 of the length toward the corner labeled "B-oxide." For example, a point in the middle of the triangle represents an oxide with the chemical formula, $ABCO_x$, where one expects 33.3% each of the A-oxide, B-oxide and C-oxide. The convex-hull formalism,[10] commonly used for thermodynamic predictions, logically derives from similar ideas.

The Cu-V-O phase space is particularly rich and the four known compounds (Table I) are shown in Figure 2b. The 1:1 compound between Bi_2O_3 and V_2O_5, positioned at the mid-point on the bottom horizontal edge in Figure 2b, is the well-studied $BiVO_4$. While not directly relevant for this review on Cu-based oxides, this particular compound is only shown in this diagram because it is a "champion" ternary oxide in terms of performance in solar water splitting.[96]

The CuO-V_2O_5 edge shows four stable ternary compounds that lie on the CuO-rich side of the edge, while the Bi_2O_3-CuO edge reveals one compound, $CuBi_2O_4$, with a 1:1 molar ratio of Bi_2O_3 and CuO. The interior of the triangle in Figure 2 represents the quaternary phase space and one specific Cu-Bi-V-O compound (the 4:1:1 ratio of CuO-Bi_2O_3-V_2O_5) is depicted in Figure 2b. Compositions beyond the quaternary case will necessitate the use of 3-D objects for visualization and their rarity puts them beyond the scope of the present discussion.

A final way to consider ternary compositions is to consider them as comprising of ionic fragments of the A cation (i.e., Cu^+ or Cu^{2+}) and the BO cluster. Indeed the compound name, in many cases, is derived by this underlying idea. To illustrate, $CuBi_2O_4$ or "copper bismuthate" (Table Ib), may be considered to be composed of Cu^{2+} and $Bi_2O_4^{2-}$ fragments. Similarly, entries #4 and #5 in Table Ib would read as "copper chromate" and "copper ferrate" respectively. There are other also more well-known such examples amongst *non-Cu* systems, e.g., bismuth titanates etc. Nonetheless, we favor the visualization based on component oxides instead, especially because the "ionic approach" is difficult to apply to quaternary cases and beyond.

Synthetic Aspects

As may be expected, a wide range of synthetic methodologies have been deployed for the preparation of ternary oxides based on Cu(I) and Cu(II). Figure 3 captures the distribution of a random sampling of these methods in the literature focusing only PEC or photocatalysis applications. Interestingly, ceramic preparation routes account for a significant number of instances in these studies. This trend is entirely in line with the theme of this review on the close relationship between solid-state chemistry and PEC. Worthy also of note is the fact that the "catch-all" (Others) category is the dominant category of methods in the Cu(II) case. This category includes variant techniques such as ion exchange, solution combustion synthesis, spin-coating, spray-pyrolysis, or metal-organic decomposition.

Given that the set of materials attributes needed for a given technological application (e.g., solar water splitting) is rather well understood,[97] it would have been ideal if a given synthesis set of conditions could be tailored a priori to yield the material with precisely those attributes. Unfortunately, this is not the case given the present state-of-the-art. The targeted attributes may even be contradictory. For example, solar energy conversion applications dictate the use of very large active material area to compensate for the diluteness of the incoming energy source (i.e., sunlight), unless of course concentrator strategies are employed. On the other hand, when nanoparticles of the active material are used, larger crystallite sizes (approaching single crystal behavior!) must be sought to minimize the role of defects and optimize carrier collection.
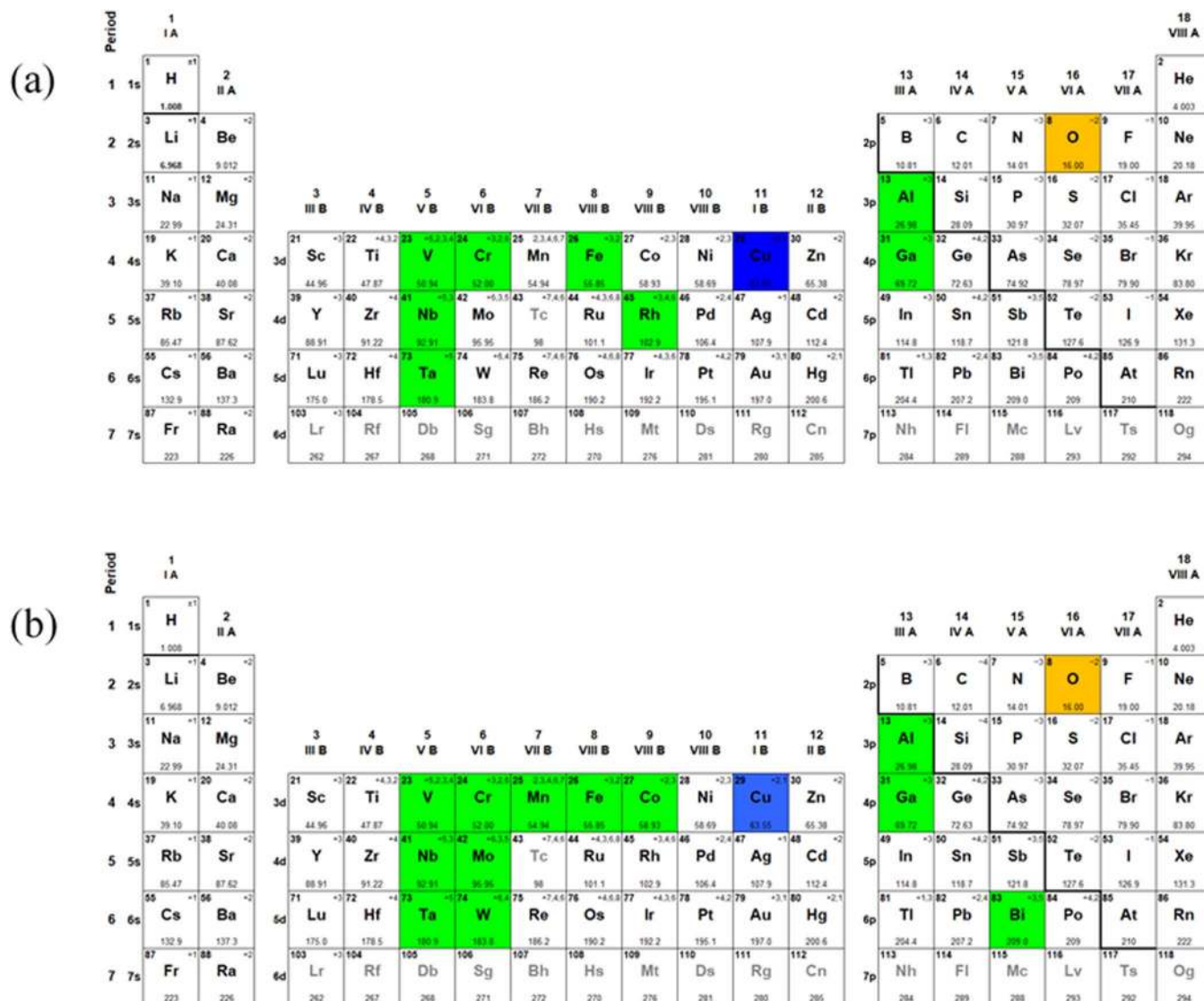
Figure 1. The ternary compounds based on Cu(I) (a) and Cu(II) (b) considered in this study and their component elements with respect to the Periodic Table (see also Tables Ia and Ib). As in the crystal structures below, the elements are color-coded, blue being the A cation (Cu) while green is the B cation in the ternary oxide compound.
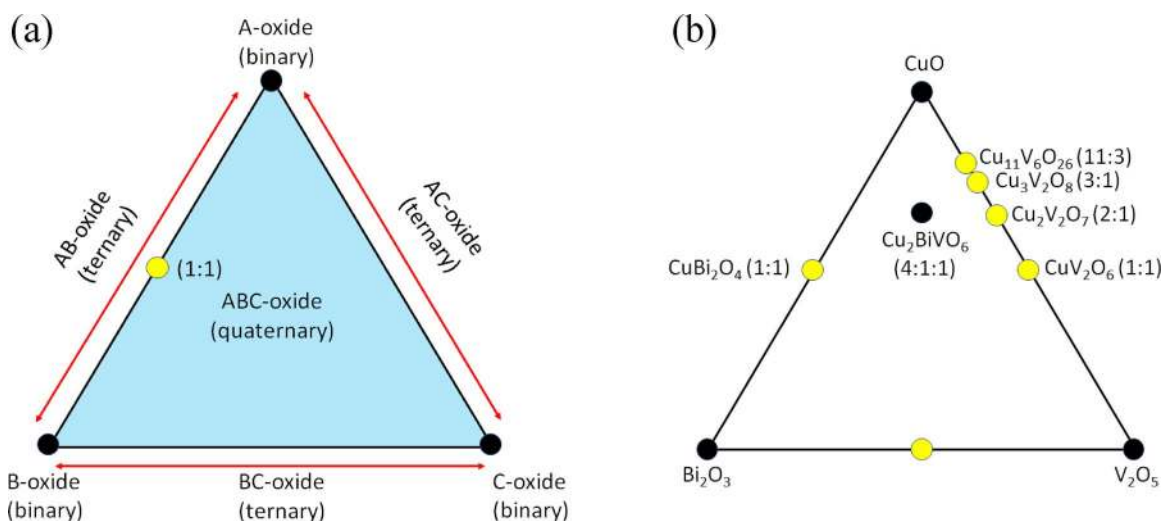

Figure 2. Graphical visualization of ternary and quaternary oxides, for the generic (a) and Bi_2O_3-CuO-V_2O_5 (b) cases.
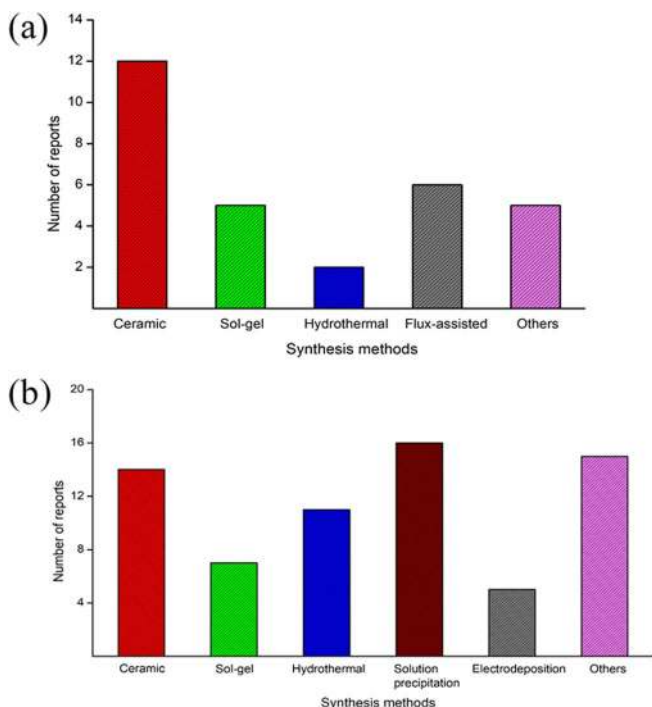
Figure 3. A sampling of the literature on PEC and photocatalysis for the examples of the choice of synthesis approaches for Cu(I) (a) and Cu(II) (b) compounds respectively. Refer also to text.

It is clear that in cases where an energy-harvesting material is to be synthesized, the energy investment for the synthesis itself, must be minimized such that the energy payback time is shortened. Solid-state (i.e., ceramic) synthesis routes are handicapped in this regard because they involve rather high temperatures. On the other hand, techniques such as solution combustion synthesis (SCS)[55,94] are attractive because the thermal energy required for the synthesis is contained within the heat of combustion of the fuel:oxidizer precursor mixture. Another important advantage of SCS is the versatility it offers for tuning the range of composition of the end product simply by varying the precursor ratio. Thus, an entire range of oxide compositions from neat CuO on the one side to the 1:1 ternary, $CuBi_2O_4$, and to Bi_2O_3 on the other, could be generated using SCS.[55] Nanocomposites containing CuO and $CuBi_2O_4$ nanoparticles in electronic contact or the $Bi_2O_3/CuBi_2O_4$ material could also be synthesized.[55] Even more significantly, SCS has also afforded the scope for preparing doped oxides or solid solutions as elaborated later in this review.

Materials discovery in its current state of evolution has to rely on either tedious trial-and error methodologies or more efficiently, the combinatorial variant. In this regard, synthesis methods that are *time-efficient* (such as SCS) hold a significant advantage over prolonged techniques (spanning several hours) such as sol-gel or solid-state routes.

Structural Aspects

Oxides display a remarkable array of structural variations that could be visualized at different levels. At the outset, we can accommodate a particular structure within a mineral type such as perovskite, spinel, delafossite etc. Another approach derives from crystallographic examination and description of the solid-state arrangement in terms of a particular space group and unit cell dimensions. A localized ("inorganic chemist's") view considers the A-O or B-O clusters that are building blocks within the overall framework and the coordination environment around the Cu cations. All three descriptions are complementary and are adopted herein, see Tables IIa and IIb for the thirty-one compounds considered in this review.

The polyhedral representations are particularly illuminating in this regard, and we begin with the structure of the perovskite prototype— a veritable "mother" of all structure types that are important in wide range of technological materials science applications. This is illustrated in Figure 4, with the Cu cation, the B cation, and the oxygens color coded the same way everywhere (c.f., Figure 1) for easy visualization. Rational and deliberate structure modifications, designed, to impart a certain characteristic (for example, a lowered optical bandgap), may be conveniently discussed with reference to this structural framework. Chemical alterations may be made either to the cationic sub-lattice or to the anionic framework (Figure 4). Thus the B cation or the oxygens in the perovskite structure may be substituted with another cation or anion with comparable ionic radii respectively. Nitrogen ($r_N = 1.5$ Å) readily substitutes for oxygen ($r_O = 1.4$ Å) affording the corresponding oxynitrides, although note that the charges are not the same in the two cases. Rational and *simultaneous* chemical alterations of this sort, targeting *both the sub-lattices*, have been reported[98] for ABO_2N type compounds, although such examples seem to be as yet sparse, for Cu-based oxides. Indeed, the so-called heteroanionic systems (e.g., oxynitrides, oxysulfides)[99,100] have garnered much interest in recent years, spurred by applications in solar fuels, thermoelectrics etc. However, these mixed *anionic* compounds are beyond the scope of the present review.

If two B cations are within ∼15% of the size of one another, a range of solid solutions may be derived with interesting gradation in structural (e.g., unit cell dimension) or optical (energy bandgap, E_g) attributes. This behavior is exemplified by the Cu-Fe-Cr-O system (Figures 5 and 6); these new materials were prepared via SCS by simple compositional tuning of the precursor mixture. Note that both the lattice parameter (a, b with black and c with blue traces in Figure 5) and E_g value (Figures 6) vary, albeit not in the same manner – the change in E_g with the extent of substitution, x being much more drastic (c.f., Figures 5b and 6b). The linear change of the lattice parameter with composition confirmed that this ternary alloy followed Vegard's law.[101]

It is worth noting that literature examples of solid solutions within the *ternary* compound space are not as common as within the *binary* compound space. Therefore, these new and interesting examples provide a guiding template for future studies on chemical composition-property relationships.

Consider now the structures of the two parents: Cu_2O and CuO (Figures 7a and 7b respectively). The unit cells are also superimposed on the ball-and-stick representation in the two cases as dotted lines. While the Cu_2O structure consists of a cubic unit cell, it is hexagonal for the CuO case. The local coordination geometry is also clearly seen to differ switching from linear in the former case to tetrahedral in the latter. Further structure details may be found for Cu_2O in a preceding review article.[6] Table II lists all the crystallographic attributes for the two parent structures as well as the 31 derivatives considered in this study.

Delafossites (Figure 8) are an important structural type for the Cu(I) case and several of these were also considered by previous authors;[6] therefore, their discussion is much abbreviated here. Interestingly, variant local coordination environments for the two cations are seen in the structural framework: linear for Cu(I) but octahedral for the B(III) cation. This structure type is observed for $CuBO_2$ (B = Rh, Fe, Al) (Table IIa). By contrast, the two cations experience a similar pyramidal coordination environment in the wurtzite structure (not shown), typical of $CuGaO_2$.

The structures of the other Cu(I) based oxides with Nb, Ta, or V as the B cation (see Table IIa) have been extensively discussed elsewhere by previous authors,[6] and therefore are not further considered here. Instead, we now turn to structures based on Cu(II): two common structure types are spinels and wolframite, shown in Figures 9a and 9b respectively. Copper-containing spinels with the general chemical formula, CuB_2O_4, have a tetragonal unit cell while Cu-containing wolframites (general formula: $CuBO_4$) possess a unit cell of much lower symmetry: either, monoclinic or triclinic, depending on the particular compound (Table IIb). Once again, the local coordination

Table II. Structural details of copper(I)- and copper(II)-based oxides.

| No.	Compound	Structure type	Crystal system	ICSD #	PDF card #	Space group	a (Å)	b (Å)	c (Å)	α (deg)	β (deg)	γ (deg)	V (Å^3)
												Cell parameters	
a) Copper(I) oxide-based													
1	$CuAlO_2$	Delafossite	Trigonal	31701	01-075-1988	$R\bar{3}m$ (166)	2.8604	2.8604	16.953	90.00	90.00	120.00	120.12
2	$CuCrO_2$	Delafossite	Trigonal	402290	01-089-6744	$R\bar{3}m$ (166)	2.9734	2.9734	17.1000	90.00	90.00	120.00	130.93
3	$CuFeO_2$	Delafossite	Trigonal	92184	01-070-6670	$R\bar{3}m$ (166)	3.03328	3.03328	17.16019	90.00	90.00	120.00	136.73
4	α-$CuGaO_2$	Delafossite	Trigonal	60846	01-077-2495	$R\bar{3}m$ (166)	2.977	2.977	17.171	90.00	90.00	120.00	131.79
5	β-$CuGaO_2$	Wurtzite	Orthorhombic	291233	-	$Pna2_1$ (33)	5.46004	6.61013	5.27417	90.00	90.00	90.00	190.35
6	$CuNbO_3$	-	Monoclinic	201899	01-084-0971	$C2/m$ (12)	9.488	8.44	6.763	90.00	90.93	90.00	541.5
7	$CuNb_3O_8$	-	Monoclinic	14099	01-071-1927	$P2_1/c$ (14)	15.365	5.0717	7.5266	90.00	107.18	90.00	560.35
8	$Cu_2Nb_8O_{21}$	-	Monoclinic	Not found in ICSD database	-	$C2/m$ (12)	10.5325	6.4306	10.173	90.00	100.212	90.00	678.11
9	$CuRhO_2$	Delafossite	Trigonal	29214	01-075-0521	$R\bar{3}m$ (166)	3.075	3.075	17.165	90.00	90.00	120.00	140.56
10	α-$Cu_2Ta_4O_{11}$	-	Monoclinic	252576	-	Cc (9)	10.7337	6.2506	12.8869	90.00	106.07	90.00	830.82
11	β-$Cu_2Ta_4O_{11}$	-	Trigonal	72179	01-081-0815	$R\bar{3}c$(167)	6.23	6.23	37.34	90.00	90.00	120.00	1255.11
12	$Cu_3Ta_7O_{19}$	-	Hexagonal	247277	-	$P6_3/m$ (176)	6.2278	6.2278	20.1467	90.00	90.00	120.00	676.71
13	$Cu_5Ta_{11}O_{30}$	-	Hexagonal	421398	01-075-2355	$P\bar{6}2c$ (190)	6.2297	6.2297	32.55	90.00	90.00	120.00	1094.00
14	Cu_3VO_4	Stannite	Tetragonal	418372	-	$I\bar{4}2\,m$ (121)	4.57531	4.57531	8.9918	90.00	90.00	90.00	188.23
b) Copper(II) oxide-based													
1	$CuAl_2O_4$	Spinel	Cubic	9558	01-071-0967	$Fd\bar{3}m$ (227)	8.078	8.078	8.078	90.00	90.00	90.00	527.12
2	$CuBi_2O_4$	Kusachiite (Spinel)	Tetragonal	71313	01-080-2489	$P4/ncc$ (130)	8.5019	8.5019	5.8196	90.00	90.00	90.00	420.65
3	$CuCo_2O_4$	Spinel	Cubic	36356	01-076-1887	$Fd\bar{3}m$ (227)	8.105	8.105	8.105	90.00	90.00	90.00	532.43
4	$CuCr_2O_4$	Spinel	Tetragonal	16708	01-072-1212	$I\bar{4}2d$ (122)	6.04	6.04	7.78	90.00	90.00	90.00	283.83
5	$CuFe_2O_4$	Spinel	Tetragonal	16666	01-072-1174	$I4_1/amd$ (141)	5.81	5.81	8.71	90.00	90.00	90.00	294.02
6	$CuGa_2O_4$	Spinel	Cubic	61028	01-078-0172	$Fd\bar{3}m$ (227)	8.298	8.298	8.298	90.00	90.00	90.00	571.37
7	$CuMn_2O_4$	Spinel	Tetragonal	9812	01-071-1142	$I4_1/amd$ (141)	5.818	5.818	8.658	90.00	90.00	90.00	293.07
8	$CuMoO_4$	-	Triclinic	22276	01-073-0488	$P\bar{1}$ (2)	9.903	6.783	8.359	101.08	96.88	107.05	517.44
9	$CuNb_2O_6$	Columbite	Monoclinic	81046	01-086-0348	$P2_1/c$ (14)	4.9991	14.1566	5.754	90.00	91.718	90.00	407.03
10	$Cu_3Nb_2O_8$	-	Triclinic	-	00-033-0476	$P\bar{1}$ (2)	5.178	5.785	6.007	100.46	83.498	65.701	148.14
11	CuV_2O_6	-	Triclinic	28151	01-074-2117	$P\bar{1}$ (2)	9.168	3.543	6.478	100.46	96.59	120.33	196.90
12	α-$Cu_2V_2O_7$	Blossite	Orthorhombic	40973	01-073-2487	$Fdd2$ (43)	20.676	8.392	6.446	90.00	90.00	90.00	1118.46
13	β-$Cu_2V_2O_7$	Ziesite	Monoclinic	158375	01-076-2820	$C2/c$ (15)	7.689	8.0289	10.1065	90.00	110.252	90.00	585.35
14	β-$Cu_3V_2O_8$	Pseudolyonsite	Monoclinic	27310	01-074-1503	$P2_1/c$ (14)	6.2493	7.9936	6.3776	90.00	111.49	90.00	296.44
15	γ-$Cu_3V_2O_8$	Mcberneyite	Triclinic	27184	01-074-1401	$P\bar{1}$ (2)	5.196	5.355	6.505	69.22	88.69	68.08	155.73
16	$Cu_{11}V_6O_{26}$	Fingerite	Triclinic	201626	01-084-0733	$P\bar{1}$ (2)	8.1576	8.2691	8.0437	107.144	91.389	106.441	493.84
17	$CuWO_4$	Distorted wolframite	Triclinic	16009	01-072-0616	$P\bar{1}$ (2)	4.7026	5.8389	4.8784	91.677	92.469	82.805	132.73
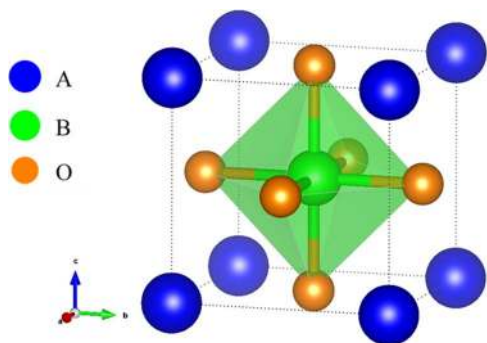
Figure 4. The perovskite structure; the unit cell is shown as a dotted line.

geometries are distinctly different for the two types of cations in the structure in both cases shown in Figures 9. In spinel structures, the Cu(II) species occupy the tetrahedral sites while the B(III) cations occupy the octahedral sites. On the other hand, both Cu(II) and B(VI) are found in octahedral geometry. Distortions from perfect geometry are common in these structures, as exemplified by $CuWO_4$.[94]

The Cu-V-O ternary system offers a remarkably diverse array of structures, particularly for the Cu(II) case. Thus the crystal structures of three Cu(II) compounds, namely, CuV_2O_6, $Cu_2V_2O_7$, and $Cu_3V_2O_8$ are shown in Figures 10–12; recall that these are the 1:1, 2:1 and 3:1 combinations of CuO and V_2O_5 (c.f., Table Ib and Figure 2b

above). Interestingly, the Cu(II) cations are in three distinctly different coordination environments in the three cases: octahedral CuO_6 in CuV_2O_6 (Figure 10a), (distorted) trigonal octahedral, CuO_5 in α-$Cu_2V_2O_7$ (Figure 11), and planar CuO_4 in γ-$Cu_3V_2O_8$ (Figures 12). By contrast, V^{5+} occurs as VO_6 or VO_4 clusters in the three cases.

Phase transitions have been studied in the Cu-V-O ternary system since the 1960s.[102,103] Polymorphs of both $Cu_2V_2O_7$ and $Cu_3V_2O_8$ are shown in Figures 11 and 12 respectively. These have been observed in recent SCS studies (as yet, unpublished) in our laboratories, and have been studied by thermal analysis and high-temperature XRD by previous authors.[102,103] Three polymorphs are known and their transitions (often reversible) occur at temperatures ranging from $\sim$500°C to $\sim$700°C. Other examples of polymorphism may be found in Table II. The wurtzite-derived β-$CuGaO_2$ structure has been studied using synchrotron X-ray radiation.[28] This structure *irreversibly* transforms to the delafossite α-phase at temperatures higher than $\sim$460°C in an Ar atmosphere.[28] In general, there is much scope for similar detailed studies on phase transitions in ternary copper oxides. It is also worth noting that the impact of these polymorphs on the corresponding optoelectronic characteristics, has not been adequately explored.

Other interesting structural questions remain, at least on a semantic level. For example, one can envision a thought experiment wherein the two component *binary* oxide structures are completely dismantled and then reassembled into a *ternary* compound framework. What dictates the ultimate crystal structure and does that have a relationship to the initial binary compound structures?
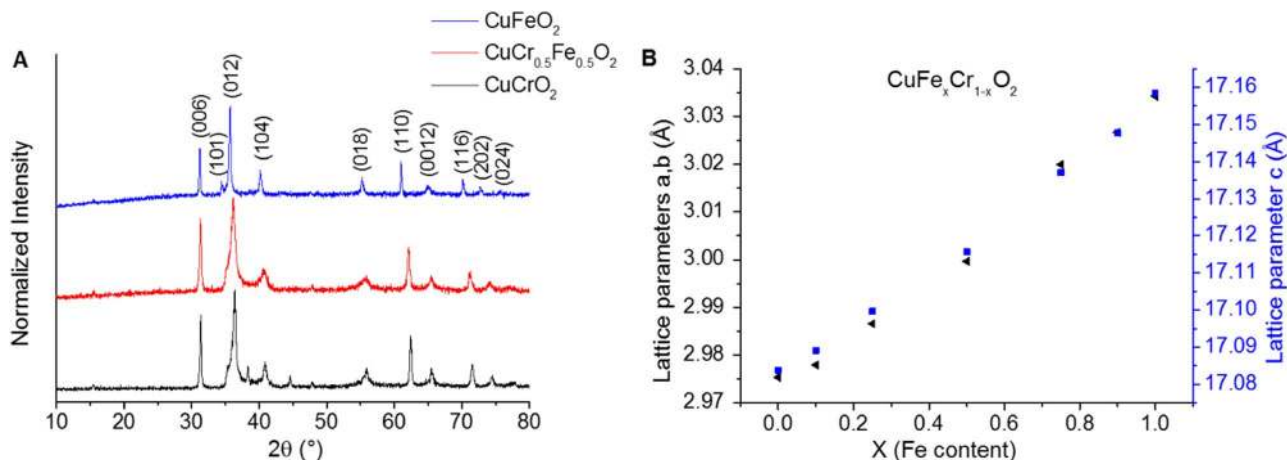

Figure 5. X-ray powder diffractograms for $CuFeO_2$, $CuCr_{0.5}Fe_{0.5}O_2$, and $CuCrO_2$ (A) Lattice parameter dependence on solid solution composition (B). (Unpublished results.).

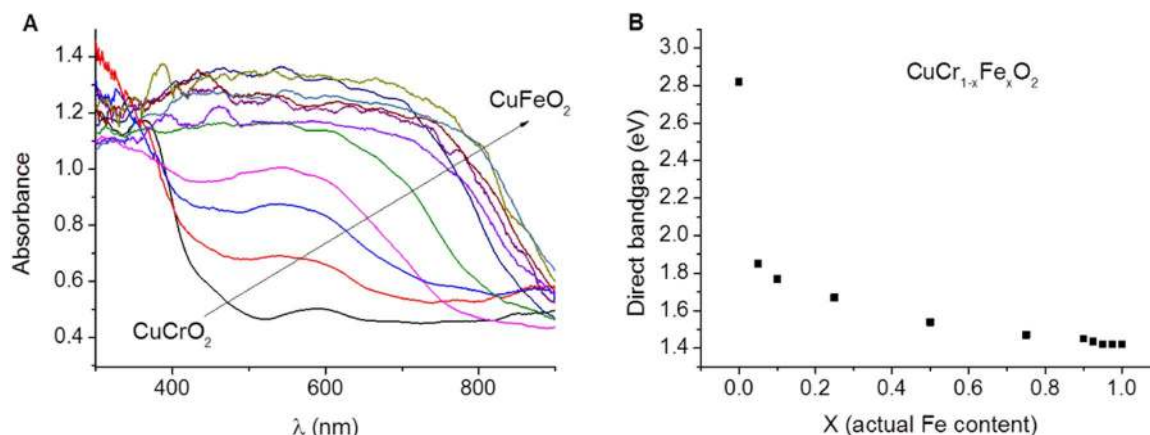**Figure 6.** UV-vis spectra for the $CuCr_{1-x}Fe_xO_2$ alloys (A). Direct bandgap values for the solid solutions (as derived from Tauc plots) and their dependence on composition (B). (Unpublished results.).
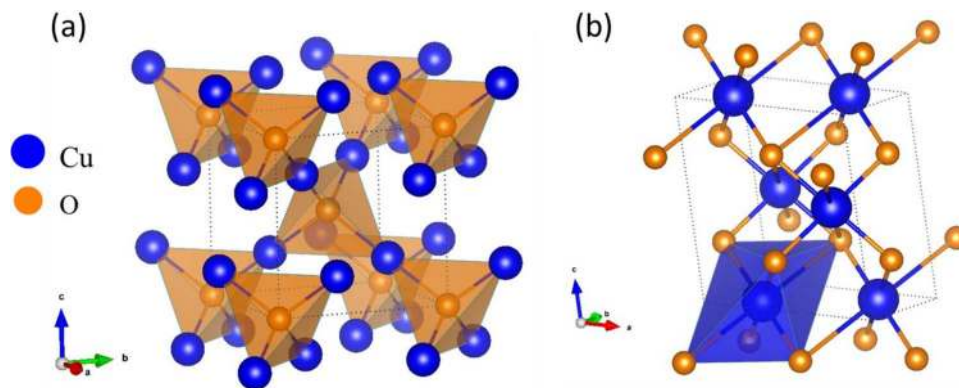
Figure 7. Crystal structures of the parent oxides: Cu$_2$O (a) and CuO (b); as in Fig. 4, the unit cells are shown as dotted lines.
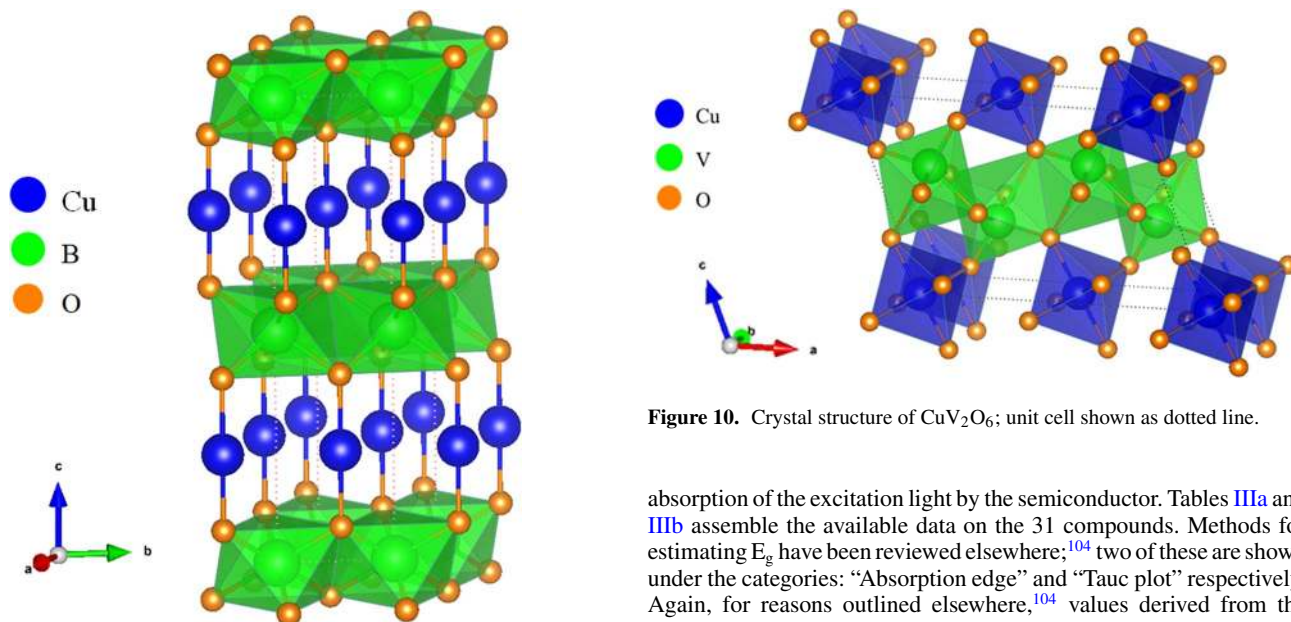

Figure 8. The delafossite crystal structure type.

Figure 10. Crystal structure of CuV$_2$O$_6$; unit cell shown as dotted line.

absorption of the excitation light by the semiconductor. Tables IIIa and IIIb assemble the available data on the 31 compounds. Methods for estimating E$_g$ have been reviewed elsewhere;[104] two of these are shown under the categories: "Absorption edge" and "Tauc plot" respectively. Again, for reasons outlined elsewhere,[104] values derived from the latter are considered to be more reliable. Nonetheless, in cases where both methods have been used, the two sets of results are in reasonable accord (see entry #2 in Table IIIb, for example). Copper tungstate and niobate are exceptions to this trend and considerable variability (as much as 1 eV or more!) exists in the reported values for reasons, again discussed elsewhere.[104] The E$_g$ values have been quoted to varying precision between 2 and 3 significant figures in Table III. Given the variability, however, only 2 significant figures may be justifiable. It is worth noting that, with rare exceptions, the vast majority of the E$_g$

Optoelectronic Aspects

Being semiconductors, an important optoelectronic property is the optical bandgap value, E$_g$. Other details on the nature of the optical transition, whether direct or indirect, has a bearing on the strength of
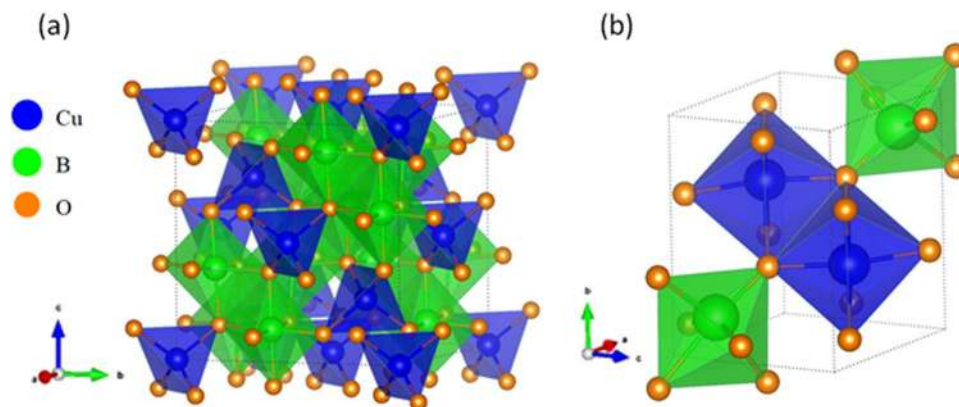

Figure 9. Crystal structures of the spinel (a) and wolframite (b) types; unit cells shown as dotted lines in both cases.
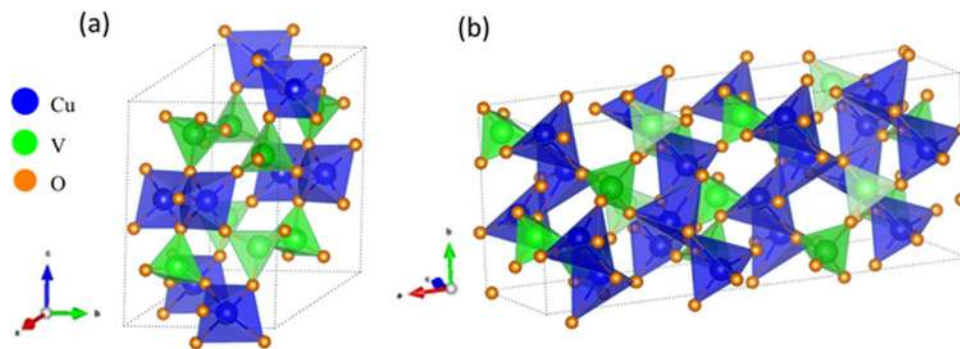
Figure 11. Crystal structures of two polymorphs of $Cu_2V_2O_7$: The β- (a) and α-modifications (b) are shown. Unit cells are shown as dotted lines.

values also lie within the "sweet spot" of optimal overlap with the solar spectrum.

Many of the compounds listed in Table III feature both types of optical transitions; therefore two separate sets of values for E_g have been listed. However, unlike in the notable case of $BiVO_4$, few questions have been raised on the nature of the fundamental bandgap in these materials. While theory can contribute much to an understanding electronic band structures, we have avoided consideration of theoretically-derived E_g values for the compilations in Table III. Accurate prediction of E_g values remains an Achilles heel of methods such as DFT, although improvements may be anticipated in the future.

As in the preceding section, interesting questions remain on the electronic nature of the resultant ternary structures after they are assembled from the binary components. Unlike in the case of solid solutions of the two components (c.f., Figure 5b), the E_g values for the ternaries are *not* bracketed by the values for the end (binary) members. Another way of looking at this is to appreciate that in many cases, the B oxide is not even a semiconductor. A case in point is entry #1 in Tables Ia and Ib above: Al_2O_3 is an insulator. In other cases, e.g., entry #7 in Table Ib, the B oxide is an electronic conductor. In most of the cases, however, the B oxide indeed is a semiconductor.

Bonding or electronic band structure theory can contribute much to an understanding of how the ternary (or higher) compound band structures involve from the binary compound cases. For example, distortions in the cation or oxygen tetrahedra have been considered as a function of the $r_{M(I)}/r_{M(III)}$ ratio in the β-$NaFeO_2$ structure (characteristic of wurtzite-derived β-$CuGaO_2$).[28] This distortion influences the energy splitting of d-orbitals in compounds containing the Cu(I) species, and in these cases, the Cu 3d orbitals strongly contribute to the top of the valence band. In general, the role of ions such as Cu^+ (or Ag^+) for that matter, as an effective electronic structure regulator, has been the topic of much recent interest in the PEC and photocatalysis communities.[105] This is because these ions affect the fundamental na-

ture of the optical transition from the valence band to the conduction band. Strategies for "optoelectronic engineering" of the band structure to intensify the light absorption strength or even the nature of the optical transition (e.g., switch from indirect to direct), are only at a rudimentary level at present. Such efforts (e.g., doping with a rare earth element) have been attempted only with binary oxides, at least to our knowledge.

Carrier transport through the semiconductor bulk follows after the initial optical excitation of the inorganic semiconductor. The dynamics of this process exerts much influence on the overall efficiency of the energy conversion or catalysis process. In most instances (unless we are considering devices of the dye-sensitized variety), it is the minority carrier diffusion length (L_D) that is the crucial parameter. The larger the L_D value is, the better is the material quality in terms of defects, traps etc. Thus for an *n*-type semiconductor, holes are the minority carriers while electrons are the minority carriers for *p*-type materials. Unfortunately, data on L_D appear to be rather sparse of the compounds considered in this review.

One exception to this trend is the Cu(II) ternary oxide, $CuBi_2O_4$. Time-resolved microwave conductivity (TRMC) and surface photovoltage (SPV) measurements were performed to assess the optoelectronic quality of this semiconductor.[52] The TRMC transient decays showed the presence of two time constants leading to L_D values of ~10 nm and ~52 nm respectively.[52] The coincidence of the SPV signal onset with the optical bandgap cut off wavelength was interpreted to signal the absence of optically active defects in the material.[52] The electrical transport mechanism has been studied and modeled as variable range small-polaron hopping at low temperatures (below 300 K) and phonon-assisted small polaron hopping at high temperatures.[106] In general, the need for more studies (both experimental and theoretical) aimed at understanding charge transport mechanism(s) in $CuBi_2O_4$, has been stressed in the literature.[52] The situation is even more pressing for the other 30 compounds in Table I.
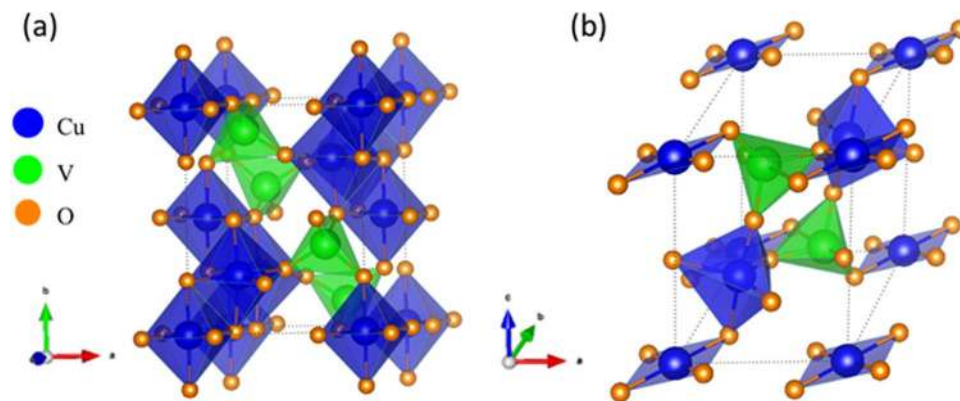

Figure 12. As in Figure 11 but for β-$Cu_3V_2O_8$ (a) and γ-$Cu_3V_2O_8$ (b). Unit cells are shown as dotted lines.

Table III. Optical bandgaps for copper oxide-based ternary oxides. a) Copper (I)-based compounds. b) Copper(II)-based compounds.

No.	Oxide	Optical bandgap (eV)			Ref. (s)
		Absorption edge	Tauc plot		
			Direct transition	Indirect transition	
a) Copper(I) oxide-based					
1	$CuAlO_2$	-	3.01	1.87	12
2	$CuCrO_2$	3.1	-	1.32	16,17
3	$CuFeO_2$	1.55	3.1	1.47	18,19
4	$\alpha\text{-}CuGaO_2$	-	3.75	2.55	22
5	$\beta\text{-}CuGaO_2$	1.47	-	-	27
6	$CuNbO_3$	-	2.09	1.89	30
7	$CuNb_3O_8$	-	-	1.26	31
8	$Cu_2Nb_8O_{21}$	-	1.6–3.0	1.43–1.65	33
9	$CuRhO_2$	1.9	-	-	34
10	$\alpha\text{-}Cu_2Ta_4O_{11}$	-	2.7	2.6	35
11	$\beta\text{-}Cu_2Ta_4O_{11}$	-	2.7	2.6	36
12	$Cu_3Ta_7O_{19}$	2.59	-	-	37
13	$Cu_5Ta_{11}O_{30}$	2.47	-	-	37
14	Cu_3VO_4	-	1.17	1.14	40
b) Copper(II) oxide-based					
1	$CuAl_2O_4$	1.77	1.8	-	41,42
2	$CuBi_2O_4$	1.4–1.8	1.48–1.80	1.42–1.84	45–55
3	$CuCo_2O_4$	-	1.49–1.74	-	58
4	$CuCr_2O_4$	-	1.40	-	66
5	$CuFe_2O_4$	-	1.24 - 1.42	-	68,69
6	$CuGa_2O_4$	-	~ 1.7	-	70
7	$CuMn_2O_4$	-	-	1.4	71
8	$CuMoO_4$	-	~ 2.8	-	72
9	$CuNb_2O_6$	-	-	1.77	74
10	$Cu_3Nb_2O_8$	2.5	-	-	75
11	CuV_2O_6	-	-	1.96	76
12	$\alpha\text{-}Cu_2V_2O_7$	-	-	1.9 ± 0.1	79
13	$\beta\text{-}Cu_2V_2O_7$	-	-	1.98	76
14	$\beta\text{-}Cu_3V_2O_8$	-	2.05–2.11	2.0–2.05	81–83
15	$\gamma\text{-}Cu_3V_2O_8$	-	2.74	1.8 ± 0.1	79,84
16	$Cu_{11}V_6O_{26}$	1.9	-	-	85
17	$CuWO_4$	-		1.8–2.4	88,90,94

Indirect insights into the optoelectronic characteristics may be gleaned from photoelectrochemical and photocatalytic activity measurements; these are considered next.

Photoelectrochemical and Photocatalytic Aspects

At the outset, it is worth mentioning that comparisons of the efficacy of a given photoelectrode (or photocatalyst powder) material with other candidates in a given application, are immediately handicapped by the absence of an agreed-upon framework for reporting PEC data or a photocatalysis figure-of-merit. This stands in contrast to photovoltaic devices where such standards exist and cell efficiencies are certified. Nonetheless, with this caveat in mind, reported data on how the 31 ternary oxides fare in either water splitting, CO_2 photoreduction, or pollutant degradation can still be made.

An immediate assessment of the photoelectrochemical quality of the oxide material may be obtained either via a photovoltammetry scan or by measuring the photocurrent at a fixed bias potential in a suitable aqueous medium.[107] For an *n*-type material, the expectation is that the photocurrent arises from the (anodic) oxidation of solution species such as water (i.e., the oxygen evolution reaction (OER). For the *p*-type material in a de-oxygenated aqueous medium, the corresponding water-splitting reaction would be the hydrogen evolution reaction or HER. Such data on 13 Cu(I)-based ternary oxides were reported by previous authors (see Table I, Ref. 6); available data on the Cu(II) counterparts are contained in Table IV.

The above assumption of the source of the photocurrent rooted in OER or HER, hinges on the fact that the extent of photoelectro-

chemical corrosion of the oxide semiconductor itself is negligible in the particular medium. This must be carefully verified by product (i.e., O_2 or H_2) collection and quantification, and comparison with the quantity expected from the charge passed (i.e., the current efficiency). In many of the cases in Table IV, this has not been done.

The other important variables in these data are the medium pH and the photon flux, both of which are specified in the compilation. Taken as a whole, $CuBi_2O_4$ is easily seen to outperform the other compounds, and the photocurrent level is at least an order of magnitude higher in this case (entry #1, Table IV).

Table V lists instances where the OER data have indeed been reported in studies on copper-based ternary oxides. The entries in this tabulation all pertain to Cu(II)-based compounds. The faradaic efficiency values indeed approach 100% except at lower bias potentials (e.g., entries # 1, 2 in Table V). Corresponding HER data are tabulated in Table VI, once again for Cu(II)-based ternary oxides. Unlike in Table V, these performance metrics pertain to *powder* suspensions of the oxide and *not* photoelectrodes. Therefore, it is more difficult to assess the efficacy in these cases, given that faradaic efficiency values, obviously, are not accessible.

Finally, CO_2 photoreduction data are summarized in Table VII; clearly, examples are rather sparse, especially for Cu(II)-based compounds. Both modes of operation, i.e., using photocathode (entry #1) or using powder suspensions (entries # 2,3) are considered in this tabulation on three ternary oxides based on Cu(II). A range of reduction products appear depending on the specific conditions used.

Table IV. Performance of Cu(II)-based ternary oxides in water splitting.

Entry No.	Oxide	Electrolytes	pH	Light source and intensity[a]	Photocurrent, $|j|/\mu A\ cm^{-2}$	Potential, V vs RHE	Semiconductor type	Comments	Ref.
1	$CuBi_2O_4$	0.3 M K_2SO_4 with 0.2 M phosphate buffer	6.65	Solar simulator	2500	0.6	*p*	-	56
2	$CuNb_2O_6$	0.1 M $NaHCO_3$ solution, bubbled CO_2	7.0	150 W tungsten–halogen	∼ 150	0.2	*p*	-	74
3	$Cu_3Nb_2O_8$	0.5 M $NaHCO_3$ solution, bubbled CO_2	7.3	Solar simulator	180	0.3	*p*	-	75
4	CuV_2O_6	0.1 M borate buffer with 0.1 M Na_2SO_3	9.2	150 W xenon lamp	∼ 220	1.58	*n*	-	76
5	$\alpha\text{-}Cu_2V_2O_7$	0.1 M borate buffer with 0.1 M Na_2SO_3	9.2	385 nm light emitting diode, illumination *power* was 3.0 mW	600	1.0	*n*	PEC was performed in scanning droplet cell.	77
6	$\beta\text{-}Cu_2V_2O_7$	0.1 M borate buffer with 0.1 M Na_2SO_3	9.2	150 W xenon lamp	∼ 120	1.58	*n*	-	76
		0.1 M borate buffer with 0.1 M Na_2SO_3	9.2	150 W xenon lamp	∼ 40	1.0	*n*	-	76
7	$\beta\text{-}Cu_3V_2O_8$	0.1 M borate buffer with 0.1 M Na_2SO_3	9.2	300 W Xe arc lamp	∼ 100	1.0	*n*	-	82
		0.1 M borate buffer with 0.1 M Na_2SO_3	9.2	300 W Xe arc lamp	∼ 150	1.0	*n*	Mo-doped sample	82
		0.1 M borate buffer with 0.1 M Na_2SO_3	9.2	300 W Xe arc lamp	∼ 100	1.0	*n*	Cr-doped sample	83
8	$\gamma\text{-}Cu_3V_2O_8$	0.1 M borate buffer with 0.1 M Na_2SO_3	9.2	150 W Xe arc	91	1.23	*n*	-	84
		0.1 M borate buffer with 0.1 M Na_2SO_3	9.2	150 W Xe arc lamp	∼ 53	1.0	*n*	-	
9	$Cu_{11}V_6O_{26}$	0.1 M borate buffer with 0.1 M Na_2SO_3	9.2	300 W Xe arc lamp	55	1.0	*n*	-	85
		0.1 M borate buffer with 0.1 M Na_2SO_3	9.2	300 W Xe arc lamp	85	1.0	*n*	Mo-doped sample	
		0.1 M borate buffer with 0.1 M Na_2SO_3	9.2	300 W Xe arc lamp	145	1.0	*n*	W-doped sample	
10	$CuWO_4$	0.1 M potassium phosphate	7.0	150 W Xe arc lamp	200	1.23	*n*	-	89

[a]The light intensity was 100 mW cm^{-2} in entries #1–4 and in #6–10.

Table V. Photoelectrochemical oxygen evolution on Cu(II)-oxides.

No.	Oxide	Medium	Light intensity	Applied potential bias (V vs RHE)	Faradaic efficiency (%)	Ref.
1	CuV_2O_6	0.1 M borate buffer, pH 9.2	300 mWcm^{-2}	1.58	70 (20 min)	77
2	$\beta\text{-}Cu_2V_2O_7$			1.58	80 (20 min)	77
3	$\beta\text{-}Cu_3V_2O_8$ (0.75 wt% Mo doped)			1.6	100 (5 min)	83
4	$Cu_{11}V_6O_{26}$ (3% Mo doped)	0.1 M borate buffer with 0.1 M Na_2SO_3, pH 9.2		1.6	95 (2 h)	86
5	$CuWO_4$	0.1 M potassium borate buffer, pH 7.0		1.23	96 (3 h)	89

Table VI. Photocatalytic HER data on Cu(II)-oxide suspensions.

No.	Oxide	Medium	Catalyst loading (g/L)	Light source	Gas evolution rate ($\mu mol\ mg^{-1}\ h^{-1}$)	Quantum yield (%)	Ref.
1	$CuAl_2O_4$	40 ml containing 0.025 M SO_3^{2-} and 1.0 M KOH	1.25	600 W tungsten lamp	0.74	0.064	44
2	$CuBi_2O_4$	100 ml 0.075 M KI solutions containing 0.05 M NaH_2PO_4/0.05 M Na_2HPO_4, pH 7.2	0.5	300 W xenon lamp	0.32	-	51
3	$CuCo_2O_4$	40 ml containing 0.025 M SO_3^{2-} and 1 M KOH	1.25	600 W tungsten lamp	1.73	0.098	44
4	$CuCr_2O_4$	40 ml containing 0.025 M $S_2O_3^{2-}$ with 0.5 M NaOH	1.25	600 W tungsten lamp	0.49	0.2	60
5	$CuFe_2O_4$	100 ml containing 0.05 M oxalic acid	1.0	250 W xenon lamp	9.0	-	67
6	$CuGa_2O_4$	250 ml of 0.5 M aqueous KOH with H_2S passed at a flow rate of 2.5 ml/min	2.0	450 W xenon lamp	3.2	5.3	70
7	$CuMn_2O_4$	40 ml containing 0.025 M SO_3^{2-} and 1 M KOH	1.25	600 W tungsten lamp	0.81	0.1	71

Corresponding reports on the use of Cu(I)-based ternaries for CO_2 photoreduction are contained in Refs. 5 and 26. A more general review on flow-based CO_2 photoreduction schemes, may be found in Ref. 108.

In general, the problems with the stability of Cu-based oxide semiconductors have been addressed by rapidly transferring the photogenerated electrons to a second phase, for example, carbon. Carbon has the advantage that the injected electrons are rapidly delocalized in the π-electron manifold. Further, many forms of nanocarbons are available. Two recent example studies on Cu_2O, may be cited.[109,110] Corresponding examples for ternary oxides are as yet lacking, at least to our knowledge.

A second type of application of inorganic oxide semiconductors is in pollutant degradation. For this environmental remediation, *n*-type semiconductors are better suited in that highly oxidizing species such as holes or hydroxyl radicals can be generated at the semiconductor-medium interface. However, the potential for *simultaneously* treating

reducible pollutants (such as toxic metal ions) also exists with heterogeneous photocatalysis, and this feature is a bonus that is not available with advanced oxidation processes (AOPs) based on ozone, H_2O_2, and the like.

Table VIII lists examples in the literature where Cu(II)-based ternary oxides have been deployed for such an application. All these examples concern the destruction of an azo dye such as methyl orange or methylene blue. While four of the reported cases show almost complete dye destruction (presumably to mineralized products), four other studies reveal only modest performance where amounts, even as low as only ~42% of the initial dye was degraded. Even the simultaneous presence of H_2O_2, as a generator of reactive oxygen species (ROS) did not seem to have helped matters to a significant extent.

The combination of optoelectronic (i.e., bandgap) data and photoelectrochemical measurements (e.g., capacitance voltage or photoaction spectroscopy) allows us to map the band edge positions

Table VII. Use of Cu(II)-based ternary oxides for CO_2 photoreduction.

			PEC CO_2 reduction				
No.	Oxide	Medium	Light intensity	Applied potential bias (V vs RHE)	Products detected	Faradaic efficiency (%)	Ref.
1	$Cu_3Nb_2O_8$	0.5 M $NaHCO_3$, pH 7.3	100 mWcm^{-2}	0.43	CO, CH_4, HCOOH, CH_3OH, C_2H_5OH and HCOH	9 (20 min)	75
			Photochemical CO_2 reduction (using suspension)				
No.	Oxide (Co-catalyst)	Medium	Catalyst loading	Light source	Product (s)	Gas evolution rate	Ref.
2	$CuCo_2O_4$ ($Ru(bpy)_3^{2+}$)	TEOA/water/ acetonitrile (1 ml/2 ml/3 ml) with 1 atm CO_2	20 mg	300 W Xe lamp	CO, H_2	22.9 $\mu mol\ h^{-1}$ CO, 5.0 $\mu mol\ h^{-1}$ H_2	57
3	$CuFe_2O_4$	300 ml containing 1.2 g KOH (1.2 gm) and 3.78 g Na_2S with pH 5.9	300 mg	500 W xenon lamp	methanol	~ 40 $\mu molg^{-1}h^{-1}$	69

Table VIII. Performance of Cu(II)-based ternary oxides in dye degradation.

No.	Oxide	Dye[a]	Dye concentration (mg/L)	Catalyst loading (g/L)	Solution volume (ml)	Irradiation time (min)	Irradiation source	Degradation (%)	Comments	Ref.
1	$CuAl_2O_4$	MO	10	3.0	50	120	125 W Hg lamp	98	-	43
2	$CuBi_2O_4$	MB	6.5	0.8	100	20	500-W Xe erc lamp	93	With added 0.1 M H_2O_2 (30 mass %)	46
3	$CuCo_2O_4$	MO	10	0.6	50	180	150 W Xe arc lamp	42	With added 0.5 mL of H_2O_2 (30 masst %)	59
4	$CuCr_2O_4$	MB	20	0.4	50	60	250 W tungsten– halogen lamp	98	With added 50 μL H_2O_2 (30%)	61
5	$CuMoO_4$	MO	10	2.0	50	60	400 W mercury lamp	72	-	72
6	β-$Cu_3V_2O_8$	MO	20	1.0	150	120	150-W Xe arc lamp	78	-	81
7	γ-$Cu_3V_2O_8$	MO	10	3.0	50	100	20 W Xe arc lamp	73	-	80
8	$CuWO_4$	MB	10	0.4	100	60	Xe arc lamp (20 mWcm^{-2})	100	With added 1 mmol H_2O_2	93

[a]MO = methyl orange; MB = methylene blue.

of the various Cu-containing ternary oxides on a common energy scale. This is shown in Figure 13; a few of these cases for the Cu(I) compounds were considered by previous authors in their review article.[6] The compilation in Figure 13 is more extensive; 24 compounds are compared here along with the two parent oxides, Cu_2O and CuO.

The thermodynamic utility of diagrams such as those in Figure 13 resides with the fact that predictions may be made for a given compound's ability to oxidize (or reduce) a targeted solution species such as water, protons, or CO_2. Since the band edges move with solution pH, it is judicious to do comparative assessments at a common pH, pH = 0 in this case.

Quaternary Oxides Based on Copper

These contain two other metal cations (B and C) besides copper in the oxide structure. One such compound, Cu_2BiVO_6, was already considered in Figure 2b earlier and consists of a 4:1:1 combination of Cu_2O, Bi_2O_3 and V_2O_5. Unlike the literature on ternary counterparts, instances where quaternary Cu-based oxides have been studied, are very sparse. This trend also contrasts with the rather rich literature on Ag-based compounds. Thus, four specific compounds appear to have been studied in the copper case: $CuAlGaO_4$,[111] Cu_2BiVO_6 (c.f., Figure 2),[112–114] and $CuBiW_2O_8$.[115] The first compound is a 2:1:1 combination of CuO, Al_2O_3, and Ga_2O_3, while the third is a 1:1:4 combination of Cu_2O, Bi_2O_3, and WO_3. These have been prepared by a diverse range of methods including solid-state synthesis,[111] chemical solution,[113] and the use of a polymeric citrate complex precursor.[112] The compounds also have been evaluated for their propensity to evolve H_2 (from H_2S),[111] O_2[114] or decompose a dye (e.g., rhodamine B)[112] under visible light irradiation. Clearly, studies on quaternary Cu-based oxides remain a fertile field of opportunity for further studies.

Concluding Remarks

Any research endeavor may be evaluated on the basis of two yard sticks: a) has it pushed the knowledge boundary forward in a transformative sense? And b) has it spawned a new technology? Recall also that the extension of the search for optimal inorganic semiconductors into the ternary (or higher) compound domain, was largely spurred by the perceived handicaps associated with the binary oxide counterparts. In the present instance, the lack of adequate photoelectrochemical stability of Cu_2O was the major driver for the search for ternary copper-based semiconductors. Are the ternary compounds more stable in a photoelectrochemical sense? The jury is still out on this aspect although there are encouraging signs that insertion of the B cation (in to the copper oxide framework) can perturb the parent electronic band structure sufficiently to stabilize the compound against photocorrosion.

Returning to the two questions posed earlier, this review demonstrates that major strides have been made in the fundamental understanding of ternary oxide semiconductors. That being said, much more must be accomplished in selected areas, and identified in the preceding sections of this article. In a practical sense, more optimization has to be done in aspects related to materials quality etc., before performance levels (e.g., photocurrents in the 10–20 mA/cm^2) can be achieved in a PEC environment (c.f., Tables IV; the maximum observed to date is 2.5 mA/cm^2, entry #1). Only then will the engineering community be motivated to tackle aspects related to photoreactor design, scale-up etc., and a viable technology emerge from all the science that would have been done up to that juncture.

Admittedly, this review has given short shrift to how theory can contribute to materials discovery, properties, and use. This reflects the authors' bias, more than anything else. Clearly, methods such as DFT (in spite of their well-recognized handicaps) and as briefly alluded to above, continue to provide much guidance to experimentalists in terms of understanding electronic band structures and their dependence on chemical composition. Although much more nascent, phase field models[116] can map morphological effects on materials properties on a mesoscale level. Such theoretical efforts could provide crucial support to the experimentalists in the continuing search and optimization of oxide semiconductors (such as the Cu-based compounds considered in this review) for solar fuels photogeneration and environmental remediation applications.
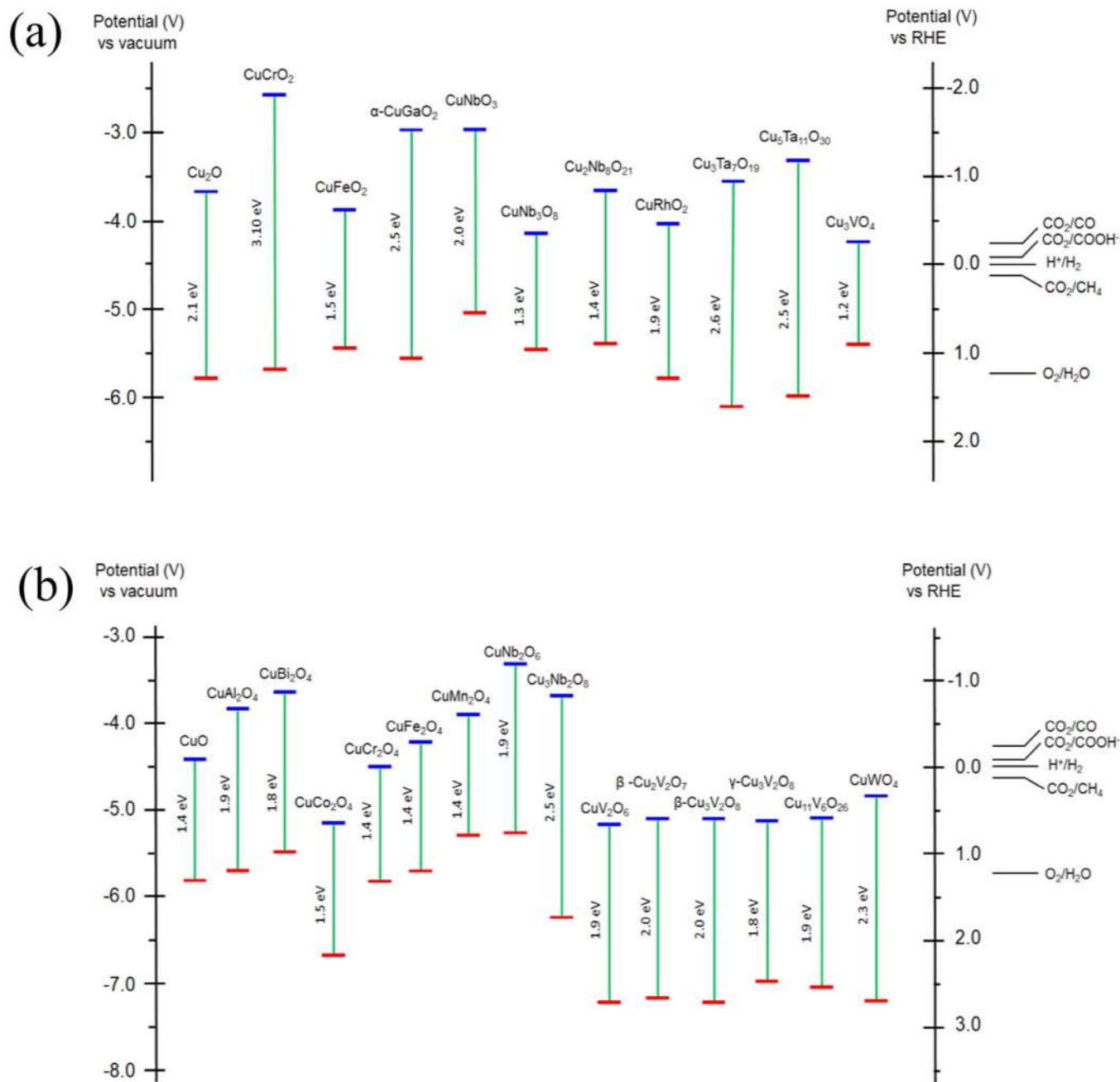
Acknowledgments

Figure 13. Band edge positions for Cu(I) (a) and Cu(II) (b) ternary oxides. Data on the parent binary oxides and relevant redox potentials are also shown for comparison.

ORCID

Krishnan Rajeshwar   https://orcid.org/0000-0003-4917-7790

References

1. A. Hamnett, M. P. Dare-Edwards, R. D. Wright, K. R. Seddon, and J. B. Goodenough, "Photosensitization of titanium(IV) oxide with tris(2,2'-bipyridine) ruthenium(II) chloride. Surface states of titanium(IV) oxide." *J. Phys. Chem.*, **83**, 3280 (1979).
2. S. Anderson, E. C. Constable, M. P. Dare-Edwards, J. B. Goodenough, A. Hamnett, K. R. Seddon, and R. D. Wright, "Chemical modification of a titanium (IV) oxide electrode to give stable dye sensitisation without a supersensitiser." *Nature*, **280**, 571 (1979).
3. H. H. Kung, H. S. Jarrett, A. W. Sleight, and A. Ferretti, "Semiconducting oxide anodes in photoassisted electrolysis of water." *J. Appl. Phys.*, **48**, 2463 (1977).
4. J. Baglio, E. Kamienieski, N. DeCola, C. Struck, J. Marzik, K. Dwight, and A. Wold, "Growth and characterization of n-WS$_2$ and niobium-doped p-WS$_2$ single crystals." *J. Solid State Chem.*, **49**, 166 (1983).
5. J. Gu, A. Wuttig, J. W. Krizan, Y. Hu, Z. M. Detweiler, R. J. Cava, and A. B. Bocarsly, "Mg-doped CuFeO$_2$ photocathodes for photoelectrochemical reduction of carbon dioxide." *J. Phys. Chem.*, **117**, 12415 (2013).
6. U. A. Joshi, A. Palasyuk, D. Arney, and P. A. Maggard, "Semiconducting oxides to facilitate the conversion of solar energy to chemical fuels." *J. Phys. Chem. Lett.*, **1**, 2719 (2010).
7. Y. Mao, T-J. Park, and S. S. Wong, "Synthesis of classes of ternary metal oxide nanostructures," *ChemComm*, 5721 (2005).

8. D. Chen, Q. Wang, R. Wang, and G. Shen, "Ternary oxide nanostructured materials for supercapacitors: a review." *J. Mater. Chem. A*, **3**, 10158 (2015).

9. W. G. Zeir, A. Zevalkink, Z. M. Gibbs, G. Hautier, M. G. Kanatzidis, and G. J. Snyder, "Thinking like a chemist: intuition in thermoelectric materials." *Angew. Chem. Int. Ed.*, **55**, 6826 (2016).

10. G. Hautier, S. P. Ong, A. Jain, C. J. Moore, and G. Ceder, "Accuracy of density functional theory in predicting formation energies of ternary oxides from binary oxides and its implication on phase stability." *Phys. Rev. B*, **85**, 155208 (2012).

11. T. F. T. Cerqueira, S. Lin, M. Amsler, S. Goedecker, S. Botti, and M. A. L. Marques, "Identification of novel Cu, Ag, and Au ternary oxides from global structural prediction." *Chem. Mater.*, **27**, 4562 (2015).

12. J. R. Smith, T. H. Van Steenkiste, and X. G. Wang, "Thermal photocatalytic generation of H$_2$ over CuAlO$_2$ nanoparticle catalysts in H$_2$O." *Phys. Rev. B*, **79**, 041403-1-4 (2009).

13. J. R. Ahmed, C. K. Blakely, J. Prakash, S. R. Bruno, M. Yu, Y. Wu, and V. V. Poltavets, "Scalable synthesis of delafossite CuAlO$_2$ nanoparticles for p-type dye-sensitized solar cells applications." *J. Alloys Compd.*, **591**, 275 (2014).

14. N. Koriche, A. Bouguelia, A. Aider, and M. Trari, "Photocatalytic hydrogen evolution over delafossite CuAlO$_2$." *Int. J. Hydrog. Energy*, **30**, 693 (2005).

15. A. Nattestad, X. Zhang, U. Bach, and Y-B. Cheng, "Dye-sensitized CuAlO$_2$ photocathodes for tandem solar cell applications." *J. Photonics Energy*, **1**, 011103-1-9 (2011).

16. C. Creissen, J. Warnan, and E. Reisner, "Solar H$_2$ generation in water with a CuCrO$_2$ photocathode modified with an organic dye and molecular Ni catalyst." *Chem. Sci*, (2018).

17. S. Saadi, A. Bouguelia, and M. Trari, "Photocatalytic hydrogen evolution over CuCrO$_2$." *Solar Energy*, **80**, 272 (2006).

18. C. G. Read, Y. Park, and K. S. Choi, "Electrochemical synthesis of p-type CuFeO$_2$ electrodes for use in a photoelectrochemical cell." *J. Phys. Chem. Lett.*, **3**, 1872 (2012).

19. M. S. Prévot, N. Guijarro, and K. Sivula, "Enhancing the performance of a robust sol–gel processed p-type delafossite CuFeO$_2$ photocathode for solar water reduction." *ChemSusChem*, **8**, 1359 (2015).

20. Y. J. Jang, Y. B. Park, H. E. Kim, Y. H. Choi, S. H. Choi, and J. S. Lee, "Oxygen-intercalated CuFeO$_2$ photocathode fabricated by hybrid microwave annealing for efficient solar hydrogen production." *Chem. Mater.*, **28**, 6054 (2016).

21. M. S. Prévot, A. X. Jeanbourquin, W. S. Bourée, F. Abdi, Friedrich D, R. Van Dr Krol, N. Guijarro, F. Le Formal, and K. Sivula, "Evaluating charge carrier transport and surface states in CuFeO$_2$ photocathodes." *Chem. Mater.*, **29**, 4952 (2017).

22. J. W. Lekse, M. K. Underwood, J. P. Lewis, and C. Matranga, "Synthesis, characterization, electronic structure, and photocatalytic behavior of CuGaO$_2$ and CuGa$_{1-x}$Fe$_x$O$_2$ (x = 0.05, 0.10, 0.15, 0.20) delafossites." *J. Phys. Chem. C*, **116**, 1865 (2012).

23. M. Yu, G. Natu, Z. Ji, and Y. Wu, "P-type dye-sensitized solar cells based on delafossite CuGaO$_2$ nanoplates with saturation photovoltages exceeding 460 mV." *J. Phys. Chem. Lett.*, **3**, 1074 (2012).

24. A. Renaud, B. Chavillon, L. Le Pleux, Y. Pellegrin, E. Blart, M. Boujtita, T. Pauporté, L. Cario, S. Jobic, and F. Odobele, "CuGaO$_2$: a promising alternative for NiO in p-type dye solar cells." *J. Mater. Chem*, **22**, 14353 (2012).

25. K. Gurunathan, J. Baeg, S. M. Lee, E. Subramanian, S. Moon, and K. Kong, "Visible light assisted highly efficient hydrogen production from H$_2$S decomposition by CuGaO$_2$ and CuGa$_{1-x}$In$_x$O$_2$ delafossite oxides bearing nanostructured co-catalysts." *Cat. Comm.*, **9**, 395 (2008).

26. H. Kumagai, G. Sahara, K. Maeda, M. Higashi, R. Abe, and O. Ishitani, "Hybrid photocathode consisting of a CuGaO$_2$ p-type semiconductor and a Ru (II)–Re (I) supramolecular photocatalyst: non-biased visible-light-driven CO$_2$ reduction with water oxidation." *Chem. Sci*, **8**, 4242 (2017).

27. T. Omata, H. Nagatani, I. Suzuki, M. Kita, H. Yanagi, and N. Ohashi, "Wurtzite CuGaO$_2$: a new direct and narrow bandgap oxide semiconductor applicable as a solar cell absorber." *J. Am. Chem. Soc.*, **136**, 3378 (2014).

28. H. Nagatani, I. Suzuki, M. Kita, M. Tanaka, Y. Katsuya, O. Sakata, S. Miyoshi, S. Yamaguchi, and T. Omata, "Structural and thermal properties of ternary narrow-gap oxide semiconductor; wurtzite-derived β-CuGaO$_2$." *Inorg. Chem.*, **54**, 1698 (2015).

29. U. A. Joshi, A. Palasyuk, and P. A. Maggard, "Photoelectrochemical investigation and electronic structure of a p-type CuNbO$_3$ photocathode." *J. Phys. Chem. C*, **115**, 13534 (2011).

30. B. Zoellner, S. Stuart, C. Chung, D. B. Dougherty, J. L. Jones, and P. A. Maggard, "CuNbTaO (x≤ 0.25) solid solutions: impact of Ta (v) substitution and Cu (I) deficiency on their structure, photocatalytic, and photoelectrochemical properties." *J. Mater. Chem. A*, **4**, 3115 (2016).

31. U. A. Joshi and P. A. Maggard, "CuNb$_3$O$_8$: a p-type semiconducting metal oxide photoelectrode." *J. Phys. Chem. Lett.*, **3**, 1577 (2012).

32. N. King, P. P. Sahoo, L. Fuoco, S. Stuart, D. Dougherty, Y. Liu, and P. A. Maggard, "Copper deficiency in the p-type semiconductor Cu$_{1-x}$Nb$_3$O$_8$." *Chem. Mater.*, **26**, 2095 (2014).

33. J. Choi, N. King, and P. A. Maggard, "Metastable Cu (I)-niobate semiconductor with a low-temperature, nanoparticle-mediated synthesis." *ACS Nano*, **7**, 1699 (2013).

34. J. Gu, Y. Yan, J. W. Krizan, Q. D. Gibson, Z. M. Detweiler, R. J. Cava, and A. B. Bocarsly, "P-type CuRhO$_2$ as a self-healing photoelectrode for water reduction under visible light." *J. Am. Chem. Soc.*, **136**, 830 (2014).

35. N. King, I. Sullivan, P. Watkins-Curry, J. Y. Chan, and P. A. Maggard, "Flux-mediated syntheses, structural characterization and low-temperature polymor-

36. N. King, R. D. Sommer, P. Watkins-Curry, J. Y. Chan, and P. A. Maggard, "Synthesis, structure, and thermal instability of the Cu$_2$Ta$_4$O$_{11}$ phase." *Cryst. Growth Des.*, **15**, 552 (2015).

37. L. Fuoco, U. A. Joshi, and P. A. Maggard, "Preparation and photoelectrochemical properties of p-type Cu$_5$Ta$_{11}$O$_{30}$ and Cu$_3$Ta$_7$O$_{19}$ semiconducting polycrystalline films." *J. Phys. Chem. C*, **116**, 10490 (2012).

38. H. Kato, A. Takeda, M. Kobayashi, M. Hara, and M. Kakihana, "Photocatalytic activities of Cu$_{3x}$La$_{1-x}$Ta$_7$O$_{19}$ solutions for H$_2$ evolution under visible light irradiation." *Catal. Sci. Technol.*, **3**, 3147 (2013).

39. I. Sullivan, P. P. Sahoo, L. Fuoco, A. Hewitt, S. Stuart, D. Dougherty, and P. A. Maggard, "Cu-deficiency in the p-type semiconductor Cu$_{5-x}$Ta$_{11}$O$_{30}$: impact on its crystalline structure, surfaces, and photoelectrochemical properties." *Chem. Mater.*, **26**, 6711 (2014).

40. P. P. Sahoo, B. Zoellner, and P. A. Maggard, "Optical, electronic, and photoelectrochemical properties of the p-type Cu$_{3-x}$VO$_4$ semiconductor." *J. Mater. Chem. A*, **3**, 4501 (2015).

41. J. Yanyan, L. Jinggang, S. Xiaotao, N. Guiling, W. Chengyu, and G. Xiumei, "CuAl$_2$O$_4$ powder synthesis by sol-gel method and its photodegradation property under visible light irradiation." *J. Sol-Gel Sci. Technol*, **42**, 41 (2007).

42. S. A. Hassanzadeh-Tabrizi, R. Pournajaf, A. Moradi-Faradonbeh, and S. Sadeghinejad, "Nanostructured CuAl$_2$O$_4$: co-precipitation synthesis, optical and photocatalytic properties." *Ceram. Int.*, **42**, 14121 (2016).

43. W. Lv, B. Liu, Q. Qiu, F. Wang, Z. Luo, P. Zhang, and S. Wei, "Synthesis, characterization and photocatalytic properties of spinel CuAl$_2$O$_4$ nanoparticles by a sonochemical method." *J. Alloys Compd.*, **479**, 480 (2009).

44. S. Saadi, A. Bouguelia, and M. Trari, "Photoassisted hydrogen evolution over spinel CuM$_2$O$_4$ (M = Al, Cr, Mn, Fe and Co)." *Renewable Energy*, **31**, 2245 (2006).

45. N. T. Hahn, V. C. Holmberg, B. A. Korgel, and C. B. Mullins, "Electrochemical synthesis and characterization of p-CuBi$_2$O$_4$ thin film photocathodes." *J. Phys. Chem. C*, **116**, 6459 (2012).

46. Y. Xie, Y. Zhang, G. Yang, C. Liu, and J. Wang, "Hydrothermal synthesis of CuBi$_2$O$_4$ nanosheets and their photocatalytic behavior under visible light irradiation." *Mater. Lett.*, **107**, 291 (2013).

47. Y. Deng, Y. Chen, B. Chen, and J. Ma, "Preparation, characterization and photocatalytic activity of CuBi$_2$O$_4$/NaTaO$_3$ coupled photocatalysts." *Alloys Compd.*, **559**, 116 (2013).

48. R. Patil, S. Kelkar, R. Naphade, and S. Ogale, "Low temperature grown CuBi$_2$O$_4$ with flower morphology and its composite with CuO nanosheets for photoelectrochemical water splitting." *J. Mater. Chem. A*, **2**, 3661 (2014).

49. Y. Nakabayashi, M. Nishikawa, and Y. Nosaka, "Fabrication of CuBi$_2$O$_4$ photocathode through novel anodic electrodeposition for solar hydrogen production." *Electrochim. Acta*, **125**, 191 (2014).

50. M. Wang, J. Zai, X. Wei, W. Chen, N. Liang, M. Xu, R. Qi, and X. Qian, "N-type hedgehog-like CuBi$_2$O$_4$ hierarchical microspheres: room temperature synthesis and their photoelectrochemical properties." *CrystEngComm*, **17**, 4019 (2015).

51. G. Sharma, Z. Zhao, P. Sarker, B. A. Nail, J. Wang, M. N. Huda, and F. E. Osterloh, "Electronic structure, photovoltage, and photocatalytic hydrogen evolution with p-CuBi$_2$O$_4$ nanocrystals." *J. Mater. Chem. A*, **4**, 2936 (2016).

52. S. P. Berglund, F. F. Abdi, P. Bogdanoff, A. Chemseddine, D. Friedrich, and R. van de Krol, "Comprehensive evaluation of CuBi$_2$O$_4$ as a photocathode material for photoelectrochemical water splitting." *Chem. Mater.*, **28**, 4231 (2016).

53. D. Cao, N. Nasori, Z. Wang, Y. Mi, L. Wen, Y. Yang, S. Qu, Z. Wang, and Y. Lei, "p-type CuBi$_2$O$_4$: an easily accessible photocathodic material for high-efficiency water splitting." *J. Mater. Chem. A*, **4**, 8995 (2016).

54. D. Kang, J. C. Hill, Y. Park, and K. S. Choi, "Photoelectrochemical properties and photostabilities of high surface area CuBi$_2$O$_4$ and Ag-Doped CuBi$_2$O$_4$ photocathodes." *Chem. Mater.*, **28**, 4331 (2016).

55. M. K. Hossain, G. F. Samu, K. Gandha, S. Santhanagopalan, J. P. Liu, C. Janáky, and K. Rajeshwar, "Solution combustion synthesis, characterization, and photocatalytic activity of CuBi$_2$O$_4$ and its nanocomposites with CuO and α;-Bi$_2$O$_3$." *J. Phys. Chem. C*, **121**, 8252 (2017).

56. F. Wang, W. Septina, A. Chemseddine, F. Abdi, D. Friedrich, P. Bogdanoff, R. van de Krol, S. Tilley, and S. Berglund, "Gradient self-doped CuBi$_2$O$_4$ with highly improved charge separation efficiency." *J. Am. Chem. Soc.*, **139**, 15094 (2017).

57. M. Jiang, Y. Gao, Z. Wang, and Z. Ding, "Photocatalytic CO$_2$ reduction promoted by a CuCo$_2$O$_4$ co-catalyst with homogeneous and heterogeneous light harvesters." *Appl. Catal. B Environ.*, **198**, 180 (2016).

58. R. Rahmatolahzadeh, M. Mousavi-Kamazani, and S. Shobeiri, "Facile co-precipitation-calcination synthesis of CuCo$_2$O$_4$ nanostructures using novel precursors for degradation of azo dyes." *J. Inorg. Organomet. Polym.*, **27**, 313 (2016).

59. S. Jeghan, J. Do, and M. Kang, "Fabrication of flower-like copper cobaltite/graphitic-carbon nitride (CuCo$_2$O$_4$/g-C$_3$N$_4$) composite with superior photocatalytic activity." *Ind. Eng. Chem. Res.*, **57**, 405 (2018).

60. S. Boumaza, R. Bouarab, Trari M, and A. Bouguelia, "Hydrogen photo-evolution over the spinel CuCr$_2$O$_4$." *Energy Convers. Manag.*, **50**, 62 (2009).

61. W. Yuan, X. Liu, and L. Li, "Synthesis, characterization and photocatalytic activity of cubic-like CuCr$_2$O$_4$ for dye degradation under visible light irradiation." *Appl. Surf. Sci.*, **319**, 350 (2014).

62. B. Paul, B. Bhuyan, D. D. Purkayastha, S. S. Dhar, and S. Behera, "Facile synthesis of spinel CuCr$_2$O$_4$ nanoparticles and studies of their photocatalytic activity in degradation of some selected organic dyes." *J. Alloys Compd.*, **648**, 629 (2015).

63. K. Mageshwari, R. Sathyamoorthy, J. Y. Lee, and J. Park, "Novel CuCr$_2$O$_4$ embedded CuO nanocomposites for efficient photodegradation of organic dyes." *Appl. Surf. Sci.*, **353**, 95 (2015).

64. F. Beshkar, O. Amiri, M. Salavati-Niasari, and F. Beshkar, "Novel dendrite-like CuCr$_2$O$_4$ photocatalyst prepared by a simple route in order to remove of azo dye in textile and dyeing wastewater." *J. Mater. Sci. Mater. Electron*, **26**, 8182 (2015).

65. L. Pan, L. Li, X. Bao, and Y. Chen, "Highly (sic) photocatalytic activity for p-nitrophenol degradation with spinel-structured CuCr$_2$O$_4$." *Micro Nano Lett*, **7**, 415 (2012).

66. H. Lahmara, M. Kebirb, N. Nasrallahb, and M. Trari, "Photocatalytic reduction of Cr(VI) on the new hetero-system CuCr$_2$O$_4$/ZnO," *J. Mol. Catal. A: Chem.*, **353**, 74 (2012).

67. H. Yang, J. Yan, Z. Lu, X. Cheng, and Y. Tang, "Photocatalytic activity evaluation of tetragonal CuFe$_2$O$_4$ nanoparticles for the H$_2$ evolution under visible light irradiation." *J. Alloys Compd.*, **476**, 715 (2009).

68. A. Kezzim, N. Nasrallah, A. Abdi, and M. Trari, "Visible light induced hydrogen on the novel hetero-system CuFe$_2$O$_4$/TiO$_2$." *Energy Convers. Manag*, **52**, 2800 (2011).

69. M. R. Uddin, M. R. Khan, M. W. Rahman, A. Yousuf, and C. K. Cheng, "Photocatalytic reduction of CO$_2$ into methanol over CuFe$_2$O$_4$/TiO$_2$ under visible light irradiation." *React. Kinet. Mech. Cat.*, **116**, 589 (2015).

70. K. Gurunathan, J. O. Baeg, S. M. Lee, E. Subramanian, S. J. Moon, and K. J. Kong, "Visible light active pristine and Fe^{3+} doped CuGa$_2$O$_4$ spinel photocatalysts for solar hydrogen production." *Int. J. Hydrog. Energy*, **33**, 2646 (2008).

71. Y. Bessekhouad and M. Trari, "Photocatalytic hydrogen production from suspension of spinel powders AMn$_2$O$_4$ (A = Cu and Zn)." *Int. J. Hydrog. Energy*, **27**, 357 (2002).

72. M. Sadeghi, "Investigation of the structural, optical and magnetic properties of CuMoO$_4$ nanoparticles synthesized through a sonochemical method." *J. Mater. Sci. Mater. Electron*, **27**, 5796 (2016).

73. T. K. Ghorai, D. Dhak, S. Dalai, and P. Pramanik, "Effect of photocatalytic activities of nano-sized copper molybdate (CuMoO$_4$)-doped bismuth titanate (Bi$_2$Ti$_4$O$_{11}$)(CMBT) alloy." *Mater Res Bull.*, **43**, 1770 (2008).

74. A. Kormányos, A. Thomas, M. N. Huda, P. Sarker, J. P. Liu, N. Poudyal, C. Janáky, and K. Rajeshwar, "Solution combustion synthesis, characterization, and photoelectrochemistry of CuNb$_2$O$_6$ and ZnNb$_2$O$_6$ nanoparticles." *J. Phys. Chem. C*, **120**, 16024 (2016).

75. S. Kamimura, N. Murakami, T. Tsubota, and T. Ohno, "Fabrication and characterization of a p-type Cu$_3$Nb$_2$O$_8$ photocathode toward photoelectrochemical reduction of carbon dioxide." *Appl. Catal. B Environ*, **174**, 471 (2015).

76. W. Guo, W. D. Chemelewski, Mabayoje O, P. Xiao, Y. Zhang, and C. B. Mullins, "Synthesis and characterization of CuV$_2$O$_6$ and Cu$_2$V$_2$O$_7$: two photoanode candidates for photoelectrochemical water oxidation." *J. Phys. Chem. C*, **119**, 27220 (2015).

77. P. F. Newhouse, D. A. Boyd, A. Shinde, D. Guevarra, L. Zhou, E. Soedarmadji, G. Li, J. B. Neaton, and J. M. Gregoire, "Solar fuel photoanodes prepared by inkjet printing of copper vanadates." *J. Mater. Chem. A*, **4**, 7483 (2016).

78. M. W. Kim, B. Joshi, H. Yoon, T. Y. Ohm, K. Kim, S. S. Al-Deyab, and S. S. Yoon, "Electrosprayed copper hexaoxodivanadate (CuV$_2$O$_6$) and pyrovanadate (Cu$_2$V$_2$O$_7$) photoanodes for efficient solar water splitting." *J. Alloys Compd.*, **708**, 444 (2017).

79. L. Zhou, Q. Yan, A. Shinde, D. Guevarra, P. F. Newhouse, N. Becerra-Stasiewicz, S. M. Chatman, J. A. Haber, J. B. Neaton, and J. M. Gregoire, "High throughput discovery of solar fuels photoanodes in the CuO–V$_2$O$_5$ system." *Adv. Energy Mater.*, **5**, 1500968 (2015).

80. M. Wang and Q. Liu, "Synthesis and photocatalytic property of Cu$_3$V$_2$O$_8$ prepared by liquid phase precipitation." *Adv Mat Res.*, **236**, 1675 (2011).

81. S. Zhang, Y. Sun, C. Li, and L. Ci, "Cu$_3$V$_2$O$_8$ hollow spheres in photocatalysis and primary lithium batteries." *Solid State Sci.*, **25**, 15 (2013).

82. J. A. Seabold and N. R. Neale, "All first row transition metal oxide photoanode for water splitting based on Cu$_3$V$_2$O$_8$." *Chem. Mater.*, **27**, 1005 (2015).

83. D. Cardenas-Morcoso, A. Peiro-Franch, I. Herraiz-Cardona, and S. Gimenez, "Chromium doped copper vanadate photoanodes for water splitting." *Cat. Today*, **290**, 65 (2017).

84. C. M. Jiang, M. Farmand, C. H. Wu, Y. S. Liu, J. Guo, W. S. Drisdell, J. K. Cooper, and I. D. Sharp, "Electronic structure, optoelectronic properties, and photoelectrochemical characteristics of γ-Cu$_3$V$_2$O$_8$ thin films." *Chem. Mater.*, **29**, 3334 (2017).

85. M. A. Lumley and K. S. Choi, "Investigation of pristine and (Mo, W)-Doped Cu$_{11}$V$_6$O$_{26}$ for use as photoanodes for solar water splitting." *Chem. Mater.*, **29**, 9472 (2017).

86. F. A. Benko, C. L. Maclaurin, and F. P. Koffyberg, "CuWO$_4$ and Cu$_3$WO$_6$ as anodes for the photoelectrolysis of water." *Mater. Res. Bull.*, **17**, 133−136 (1982).

87. J. P. Doumerc, J. Hejtmanek, J. P. Chaminade, M. Pouchard, and M. Krussanova, "A Photoelectrochemical study of CuWO$_4$ single crystals." *Phys. Stat. Sol.*, **82**, 285−294 (1984).

88. J. E. Yourey, K. J. Pyper, J. B. Kurtz, and B. M. Bartlett, "Chemical stability of CuWO$_4$ for photoelectrochemical water oxidation." *J. Phys. Chem. C*, **117**, 8708−8718 (2013).

89. J. E. Yourey and B. M. Bartlett, "Electrochemical deposition and photoelectrochemistry of CuWO$_4$, a promising photoanode for water oxidation." *J. Mater. Chem.*, **21**, 7651−7660 (2011).

90. Y. Chang, A. Braun, A. Deangelis, J. Kaneshiro, and N. Gaillard, "Effect of thermal treatment on the crystallographic, surface energetics, and photoelectrochemical properties of reactively co-sputtered copper tungstate for water splitting." *J. Phys. Chem. C*, **115**, 25490−25495 (2011).

91. Y. Tang, N. Rong, F. Liu, M. Chu, H. Dong, Y. Zhang, and P. Xiao, "Enhancement of the photoelectrochemical performance of CuWO$_4$ films for water splitting by hydrogen treatment." *Appl. Surf. Sci.*, **361**, 133−140 (2016).

92. Y. Gao, O. Zandi, and T. W. Hamann, "Atomic layer stack deposition-annealing synthesis of CuWO$_4$." *J. Mater. Chem. A*, **4**, 2826−2830 (2016).

93. X. Xie, M. Liu, C. Wang, L. Chen, J. Xu, Y. Cheng, H. Dong, F. Lu, W. H. Wang, H Liu, and W. Wang, "Efficient photo-degradation of dyes using CuWO$_4$ nanoparticles with electron sacrificial agents: a combination of experimental and theoretical exploration." *RSC Adv.*, **6**, 953 (2016).

94. A. Thomas, C. Janáky, G. F. Samu, M. N. Huda, P. Sarker, J. P. Liu, V. Van Nguyen, E. H. Wang, K. A. Schug, and K. Rajeshwar, "Time and energy-efficient solution combustion synthesis of binary metal tungstate nanoparticles with enhanced photocatalytic activity." *ChemSusChem.*, **8**, 1652 (2015).

95. N. R. de Tacconi, H. K. Timmaji, W. Chanmanee, M. N. Huda, P. Sarker, C. Janaky, and K. Rajeshwar, "Photocatalytic generation of syngas using combustion-synthesized silver bismuth tungstate." *ChemPhysChem*, **13**, 1 (2012).

96. J. K. Cooper, S. Gul, F. M. Toma, L. Chen, Y-S. Liu, J. Guo, J. W. Ager, J. Yano, and I. D. Sharp, "Indirect bandgap and optical properties of monoclinic bismuth vanadate." *J. Phys. Chem. C*, **119**, 2969 (2015). See also references therein.

97. K. Watanabe, "Photocatalytic water splitting: Quantitative approaches toward photocatalyst by design," *ACS Catal.*, **7**, 8006 (2017).

98. A. Maegli, E. H. Otal, T. Hisatomi, S. Yoon, C. M. Leroy, N. Schauble, Y. Lu, M. Gratzel, and A. Weidenkaff, "Perovskite-type LaTiO$_2$N oxynitrides for solar water splitting: Influence of the synthesis conditions, " *Energy Procedia* **22**, 61 (2012).

99. K. Sivula and R. van De Krol, "Semiconducting materials for photoelectrochemical energy conversion," *Nat. Rev. Mater.*, **1**, 1 (2016).

100. K. Rajeshwar, in *Solar Hydrogen Generation: Toward a Renewable Energy Future*, (edited by K. Rajeshwar, R. McConnell, and S. Licht,), Chapter 7, pp. 167, Kluwer Academic, New York (2008).

101. L. Vegard, "Die konstitution der mischkristalle und die raumfüllung der atome," *Zeitschrift Für Phys.*, **5**, 17.

102. G. M. Clark and R. Garlick, "Formation and properties of copper(I) divanadate(V)," *J. Inorg. Nucl. Chem.*, **40**, 1347 (1978). See also references therein.

103. N. S. Rao and O. G. Palanna, "Phase transitions in copper(II) orthovanadate," *Bull. Mater. Sci.*, **16**, 261 (1993).

104. D. Roy, G. F. Samu, M. K. Hossain, C. Janaky, and K. Rajeshwar, "On the measured optical bandgap values of inorganic oxide semiconductors for solar fuels generation," *Catal. Today*, **300**, 136 (2018).

105. For example: H. Dong, G. Chen, J. Sun, C. Li, Y. Hu, and Z. Han, "Whole-visible-light (sic) absorption of a mixed-valence silver vanadate semiconductor stemming from an assistant (sic) effect of d-d transition," *Inorg. Chem.*, **54**, 11826 (2015). See also references therein.

106. S. Hazra, S. Mandal, and A. Ghosh, "Transport mechanism in nonconventional bismuth cuprate glass," *J. Chem. Phys.*, **104**, 10041 (1996).

107. K. Rajeshwar, in *Encyclopedia of Electrochemistry*, (edited by S. Licht,), Chapter 1, pp. 3, Wiley-VCH, Weinheim (2001).

108. B. Endrodi, G. Bencsik, F. Darvas, R. Jones, K. Rajeshwar, and C. Janaky, "Continuous –flow electroreduction of carbon dioxide," *Prog. Energy Combustion Sci.* **62**, 133 (2017).

109. E. Kecsenovity, B. Endrődi, Z. Pápa, K. Hernádi, K. Rajeshwar, and C. Janáky, "Decoration of ultralong carbon nanotubes with Cu$_2$O nanocrystals: a hybrid platform for enhanced photoelectrochemical CO$_2$ reduction," *Journal of Materials Chemistry A*, **4**, 3139 (2016).

110. E. Kecsenovity, B. Endrődi, P. S. Tóth, Y. Zou, R. A. W. Dryfe, K. Rajeshwar, and C. Janáky, "Enhanced photoelectrochemical performance of cuprous-oxide/graphene nanohybrids," *Journal of the American Chemical Society*, **139**, 6682 (2017).

111. S. K. Biswas, J-O. Baeg, B. B. Kale, R. K. Yadav, S-J. Moon, K-J. Kong, and W-W. Soo, "An efficient visible-light active photocatalyst CuAlGaO$_4$ for solar hydrogen production," *Catal. Commun.*, **12**, 651 (2011).

112. Z. Ding, Y. Fu, Z. Xie, and Z. Li, "A polymeric complex method to nanocrystalline BiCu$_2$VO$_6$ with visible light photocatalytic activity," *Mater. Lett.*, **65**, 460 (2011).

113. Y. Nakabayashi, M. Nishikawa, and Y. Nosaka, "Fabrication of bismuth copper vanadate electrodes through feasible chemical solution method for visible light-induced water oxidation," *J. Appl. Electrochem.*, **46**, 9 (2015).

114. H. Liu, R. Nakamura, and Y. Nakato, "Bismuth-copper vanadate BiCu$_2$VO$_6$ as a novel photocatalyst for efficient visible light driven oxygen evolution," *ChemPhysChem*, **6**, 2499 (2005).

115. P. Sarker, D. Prasher, N. Gaillard, and M. N. Huda, "Predicting a new photocatalyst and its electronic properties by density functional theory," *J. Appl. Phys.*, **114**, 133508 (2013).

116. For example, Y. Cao, J. Shen, C. Randall, and L-Q. Chen, "Effect of multi-domain structure on ionic transport, electrostatics, and current evolution in BaTiO$_3$ ferroelectric capacitor," *Acta Mater.*, **112**, 224 (2016). See also references therein.